Journal of Computational Applied Mechanics 2024, 55(4): 744-770

DOI: 10.22059/jcamech.2024.380432.1183

RESEARCH PAPER

Geometrical assessment of rectangular fins at different surfaces and positions on Nusselt number of lid-driven cavities under laminar forced convection

Eliciana Sias Aldrighi [a], Giulio Lorenzini [b,*], Giovani Dambros Telli [c], Flávia Schwarz Franceschini Zinani [d], Liércio André Isoldi [a], Luiz Alberto Oliveira Rocha [a,e,f], Elizaldo Domingues dos Santos [a,e]

[a] *Graduate Program in Computational Modeling, Universidade Federal do Rio Grande, Itália Avenue, km 8, 96201-900, Rio Grande, Brazil*
[b] *Department of Engineering and Architecture, University of Parma, Parco Area delle Scienze, 181/A, 43124, Parma, Italy*
[c] *Área do Conhecimento de Ciências Exatas e Engenharias, Universidade de Caxias do Sul, Rua Francisco Getúlio Vargas 1130, 95070-560, Caxias do Sul, Brazil*
[d] *Institute of Hydraulic Research, Universidade Federal do Rio Grande do Sul (IPH-UFRGS), Av. Bento Gonçalves 9500, 91501-970, Porto Alegre, Brazil*
[e] *Institute of Earth Sciences, Complex Fluid Systems Lab, Rua Romao Ramalho 59, 7000-671 Evora, Portugal*
[f] *Mechanical Engineering Graduate Program, Universidade Federal do Rio Grande do Sul – UFRGS, Rua Sarmento Leite 425, 90040-001 Porto Alegre, Brazil*

Abstract

This work focused on the geometric assessment by the lens of the Constructal Design of a rectangular fin placed at different surfaces and positions of lid-driven cavities under laminar forced convection. This study aims to maximize the Nusselt number (Nu_H) from the isothermal fin for Reynolds numbers (Re_H) ranging from 10 to 1000 and a fixed Prandtl equal to 0.71. The fin was placed at the lower, upstream, and downstream cavity surfaces in five positions (S^* = 0.1; 0.3; 0.5; 0.7; 0.9). The domain presents two constraints: the cavity area and the ratio fin area to cavity area kept constant for all cases (φ = 0.05). The degrees of freedom explored to maximize the Nusselt number were the ratio between the height and length of the fin (H_1/L_1) and the fin position along each cavity surface. The results indicated that the fin geometry and positions significantly affected the Nusselt number. The highest Nusselt number was achieved for the fin positioned on the downstream cavity surface with H_1/L_1 = 2.0 and S^* = 0.9, improving the Nusselt number by 63.1% and 5.8% compared to the optimal shapes in the lower and upstream cavity surfaces.

Keywords: Rectangular fins; lid-driven cavity; numerical study; forced convection; constructal design;

* Corresponding author. Tel.: +39 0521 902111
E-mail address: giulio.lorenzini@unipr.it

Nomenclature

A	Domain area (channel)	m²
A_f	Area filled by the fin in cavity	m²
cp	Specific heat at constant pressure	J/(kg.K)
h	Convection heat transfer coefficient	W/(m².K)
H	Cavity height	m
H_1	Height of rectangular fin	m
k	Thermal conductivity of the fluid	W/(m.K)
L	Cavity length	m
L_1	Length of the rectangular fin	m
NuH	Nusselt number for characteristic height	-
P	Pressure	N/m²
Pr	Prandtl number	-
ReH	Reynolds number	-
Ri	Richardson number	-
S^*	Position of the fin in the cavity surface	-
T_i	Initial temperature	K
T_s	Temperature of the top surface of the cavity	K
T_f	Temperature of the fin surface	K
x	Spatial coordinate in horizontal direction	m
y	spatial coordinate in vertical direction	m
Greek symbols		
μ	Dynamic viscosity	kg/(m.s)
ρ	Density	kg/m³
ϕ	Fraction of the area filled by the fin and the cavity area	
Subscripts		
m	Once maximized	
mm	Twice maximized	
o	Once optimized	
oo	Twice optimized	

1. Introduction

Heat transfer systems have been miniaturized nowadays, particularly in electronic components, making developing more effective cooling solutions an intriguing research area. The convective heat transfer process in cavity flows has become a subject of extensive research due to its relevance in various engineering applications, such as heat exchangers, gas turbines, electronic systems, and microelectronic chips [1]. The complexity of fluid dynamics within these cavities, coupled with the presence of inserted fins or obstacles, presents a challenging but promising area for investigation. The internal flow in lid-driven cavities is an ideal case for studying fluid behaviour due to its simplicity in geometry but rich complexity in physics phenomena [2]. Key features of this flow include the development of primary vortices, reattachment and separation of boundary layers, and the potential emergence of secondary vortices, especially at high Reynolds numbers [3]. Furthermore, the mixed convection mechanism governs the heat transfer process in lid-driven cavities. Forced convection occurs via the movement of the shear flow created by the lid-driven wall, whereas natural convection is caused by the buoyancy flow created due to temperature gradients [4, 5]. Thus, understanding the intricate interplay between fluid flow, heat transfer, and geometric configurations is crucial for designing more efficient thermal management systems.

In this regard, internal flows within cavities have been extensively researched to understand the thermal-fluid dynamics of forced convection [6 – 8] and mixed convection [9 – 11]. The effect of several cavity shapes, such as rectangular and trapezoidal, on the thermal-fluid domain has been studied in the literature [12 – 16]. Moallemi and

Jang [12] explored the impact of the Prandtl number on the thermal performance of mixed convection in lid-driven square cavities. They found that the impacts of buoyancy flow were noticeable with higher Prandtl values. A mixed convection in a rectangular cavity was studied by [13]. The findings showed that changes in the Richardson number (*Ri*) influenced heat transfer.

Studies that evaluate mounted fins or obstacles inside cavities have been explored in the literature. Chamkha et al. [17] studied the influence of cavity geometry, Reynolds, and Richardson numbers on the thermal performance of a heated square cylinder under mixed convection in a square-vented cavity. Oztop et al. [18] also studied a heated cylinder inserted in a square cavity under mixed convection. It was reported that once the cylinder's diameter is small, thermal conductivity does not affect the solution. However, the Nusselt number (*Nu*) increases as the body's diameter increases. Gibanov et al. [19] studied the mixed convection heat transfer process in a cavity with a bottom heat-conducting solid backward step. The authors varied the geometry of the solid form and evaluated the heat transfer process. They reported that varying the size and thermal conductivity of the backward step modified the flow and heat transfer patterns. In another work, a rotating cylinder inside a lid-driven cavity was studied in reference [20]. Results indicated that the Nusselt number tends to increase with the increase in the cylinder's rotating velocity for different *Ri* numbers. Other works in the literature also explored rotating cylinders inside lid-driven cavities [16, 21, 22]. Gangaware et al. [10] examined a triangular block inserted in a lid-driven cavity. A constant heat flux was applied to the triangular block, changing its position in the cavity. The results indicated that the highest heat transfer rates were achieved for the triangular block in the middle of the cavity. In addition, the *Nu* decreased with the increase in the *Ri* number. Moayedi et al. [23] explored four distinct fin geometries (T, Y, Γ and ㄱ) in a lid-driven square cavity under mixed convection. The study found that altering the fin geometry from T to Γ improved the Nusselt number.

The geometry of the mounted fins or obstacles can alter the flow patterns, disrupt boundary layers, and facilitate convective heat transfer, thus offering opportunities for improving thermal performance. Moreover, the position of these fins or obstacles within the cavity is important to the overall heat transfer efficiency. One possible method to evaluate the design and position of the inserted fins or obstacles inside a lid-driven cavity is applying the Constructal Design method, which is based on the Constructal Law. The Constructal Law was postulated by Bejan [24] and describes the natural trend of any flow systems to evolve over time to ease access to the internal streams flowing through them [25 – 27]. The design modifications occur to reduce the thermodynamic imperfections present in all flow systems [28 – 30]. The Constructal Design approach may be used in various research topics, such as in the vascular blood flow structure in a liver [31] or in the formation of trees and river basins [26]. In engineering applications, advances have been proposed using the Constructal Design in the growth of capillary networks [32], latent and sensible heat exchangers [33, 34], the design of battery thermal management systems [35, 36], heat dissipating structures [37], and cooling of electronic packaging or integrated circuits [38, 39]. It is clear from these examples that the modifications in the flow configuration are a key aspect of more efficient systems.

Recently, the Constructal Design approach has been used to study the geometry of fins and obstacles inserted in lid-driven cavities to enhance the heat transfer performance of these systems. Lorenzini et al. [40] explored the thermal performance of rectangular fins inserted in the middle of the low surface of the lid-driven square cavity under mixed convection. They explored different fins aspect ratios, Rayleigh, and Reynolds numbers. Similarly, Aldrighi et al. [41] investigated the heat transfer process for different rectangular fin geometries inserted in the centre of distinct surfaces of a lid-driven cavity flow under forced convection. Rodrigues et al. [5] studied the mixed convection heat transfer process of two rectangular intrusions in a lid-driven cavity. Both rectangular fins were placed at the inferior of the cavity's surface. The authors varied the aspect ratio of the two inserted fins and the Richardson number for a constant Reynolds number equal to 400 and Pr = 6.0. Razera et al. [42] evaluated the thermal performance of mixed convection with different semi-elliptical fin geometries mounted in a lid-driven square cavity. The semi-elliptical fin was positioned in the middle of each cavity's surface. The authors explored different semi-elliptical fin geometries for several Rayleigh and Reynolds numbers. Borahel et al. [43] investigated different geometries for a rectangular isothermal block (IB) inside a lid-driven cavity to enhance the thermal performance of the system. The authors studied rectangular isothermal block geometries for different IB/cavity area fractions and Richardson numbers.

This work introduces a geometrical assessment of a rectangular fin mounted on different surfaces and positions of lid-driven cavities under laminar forced convective flows. This study investigates the relation of the height and length of the fin (H_1/L_1) under the Constructal Design lens to enhance the heat transfer performance of the system. The fin is inserted in three distinct cavity surfaces - low, downstream, and upstream surfaces - and on each surface, the fin is placed in five different positions (S^* = 0.1; 0.3; 0.5; 0.7; 0.9). Furthermore, the influence of the Reynolds number ($10 \leq Re_H \leq 1000$) on the Nusselt number in the heated fin and fluid flow and the optimal fin shapes were also addressed. The study was carried out with a constant relation of the area filled by the fin and cavity area of φ = 0.05, and constant Prandtl number (Pr = 0.71). It is important to highlight that the combined conditions evaluated in this work have not been investigated yet in Refs. [40 – 41]. The novelty of this work is based on the rectangular fin with variable aspect ratio placed in five different positions in the cavity surface's low, upstream and downstream boundaries, which was not previously investigated. As a result, this study aims to provide a novel contribution to the scientific field of lid-driven cavity flows using the constructal design method.

2. Mathematical modelling

This work numerically evaluates the flow and heat transfer in lid-driven square cavities with rectangular fins. The flow is assumed incompressible, laminar, and steady state. Fig. 1 shows the problem domain, representing boundary conditions and geometrical variables. The fin was placed at the low surface (LS) (a), the downstream surface (DS) (b), and the upstream surface (US) (c), as presented in Fig. 1. The cavity was modeled as a two-dimensional domain with H = L= 1 m. The fluid inside the cavity had constant thermal physical properties. The modeling equations for the fluid domain are the mass, momentum and energy balance equations, given as [44]:

$$\frac{\partial u}{\partial x}+\frac{\partial v}{\partial y}=0 \tag{1}$$

$$\rho\left(u\frac{\partial u}{\partial x}+v\frac{\partial u}{\partial y}\right)+\frac{\partial P}{\partial x}-\mu\left(\frac{\partial^2 u}{\partial x^2}+\frac{\partial^2 u}{\partial y^2}\right)=0 \tag{2}$$

$$\rho\left(u\frac{\partial v}{\partial x}+v\frac{\partial v}{\partial y}\right)+\frac{\partial P}{\partial y}-\mu\left(\frac{\partial^2 v}{\partial x^2}+\frac{\partial^2 v}{\partial y^2}\right)=0 \tag{3}$$

$$\rho C_p\left(u\frac{\partial T}{\partial x}+v\frac{\partial T}{\partial y}\right)-k\left(\frac{\partial^2 T}{\partial x^2}+\frac{\partial^2 T}{\partial y^2}\right)=0 \tag{4}$$

where x and y are the Cartesian spatial coordinates, u and v are the velocity components in x and y directions, P is the pressure; T is the temperature, ρ is the density, μ is the dynamic viscosity, Cp is the specific heat, and k is the thermal conductivity.

The problem's variables can be stated in a dimensionless form to generalize the results. Dimensionless parameters are represented by the asterisk, and given as:

$$x^*, y^*, H^*, L^*, H_1^*, L_1^* = \frac{x, y, H, L, H_1, L_1}{A^{1/2}} \tag{5}$$

$$u^*, v^* = \frac{u, v}{u_0} \tag{6}$$

$$T^* = \frac{T - T_{\min}}{T_{\max} - T_{\min}} \tag{7}$$

where A is the cavity area, u_0 is the velocity imposed at the cavity lid, $T_{\min}$ is the temperature at the cavity lid and $T_{\max}$ is the temperature of the fin surfaces.

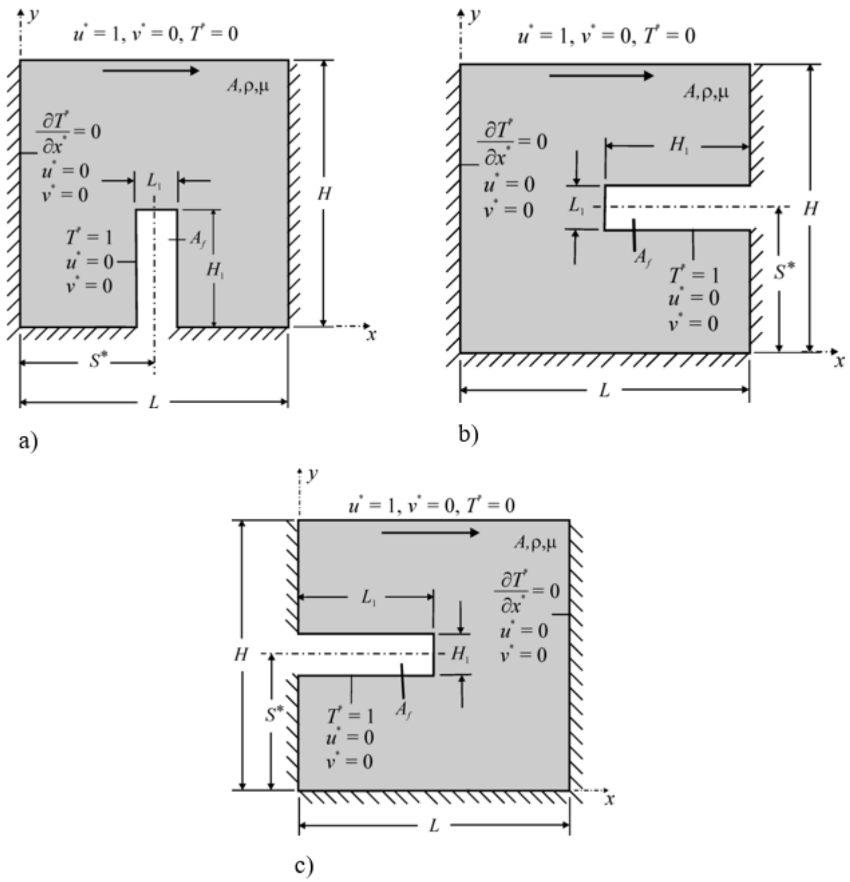

Fig 1: Problem statement for the flow inside cavities with rectangular fin at different surfaces: a) low, b) downstream, c) upstream.

The fluid flow is driven by the continuous displacement of the upper surface of the cavity (forced convection), as illustrated in Fig. 1. The Reynolds number was calculated using the upper surface velocity, u_0, as a reference. The upper surface has a dimensionless velocity of $u^* = 1$ and $v^* = 0$. On the other surfaces, lateral and bottom, the velocities are dimensionless and prescribed as zero ($u^* = v^* = 0$) with nonslip and impermeability conditions. Regarding the thermal boundary conditions, the bottom and lateral of the cavity were considered adiabatic (thermally insulated). In this model, the flow is heated by surfaces of the fin, which have a dimensionless temperature of $T^* = 1.0$, while the cavity top surface temperature is considered as $T^* = 0$. The Prandtl number was assumed constant during the simulations ($Pr = 0.71$).

This investigation aimed to find the configurations that give the greatest Nusselt number between the fin and the surrounding fluid. Thus, the Constructal Design method has been applied to define the flow system, performance indicator, degrees of freedom, and restrictions in investigating fin's geometries [24 – 27, 5, 43]. Fig. 2 shows a flowchart illustrating the main steps to achieve the objectives of the current study.

As shown in Fig. 2, the geometry is constrained by two variables: the cavity's area (A) and the area filled by the fin within the cavity (A_f). These variables are given by the following equations:

$$A = HL \tag{8}$$

$$A_f = H_1 L_1 \tag{9}$$

where H are the height and L are the length of the square cavity, H_1 and L_1 are the height and length of the rectangular fin.

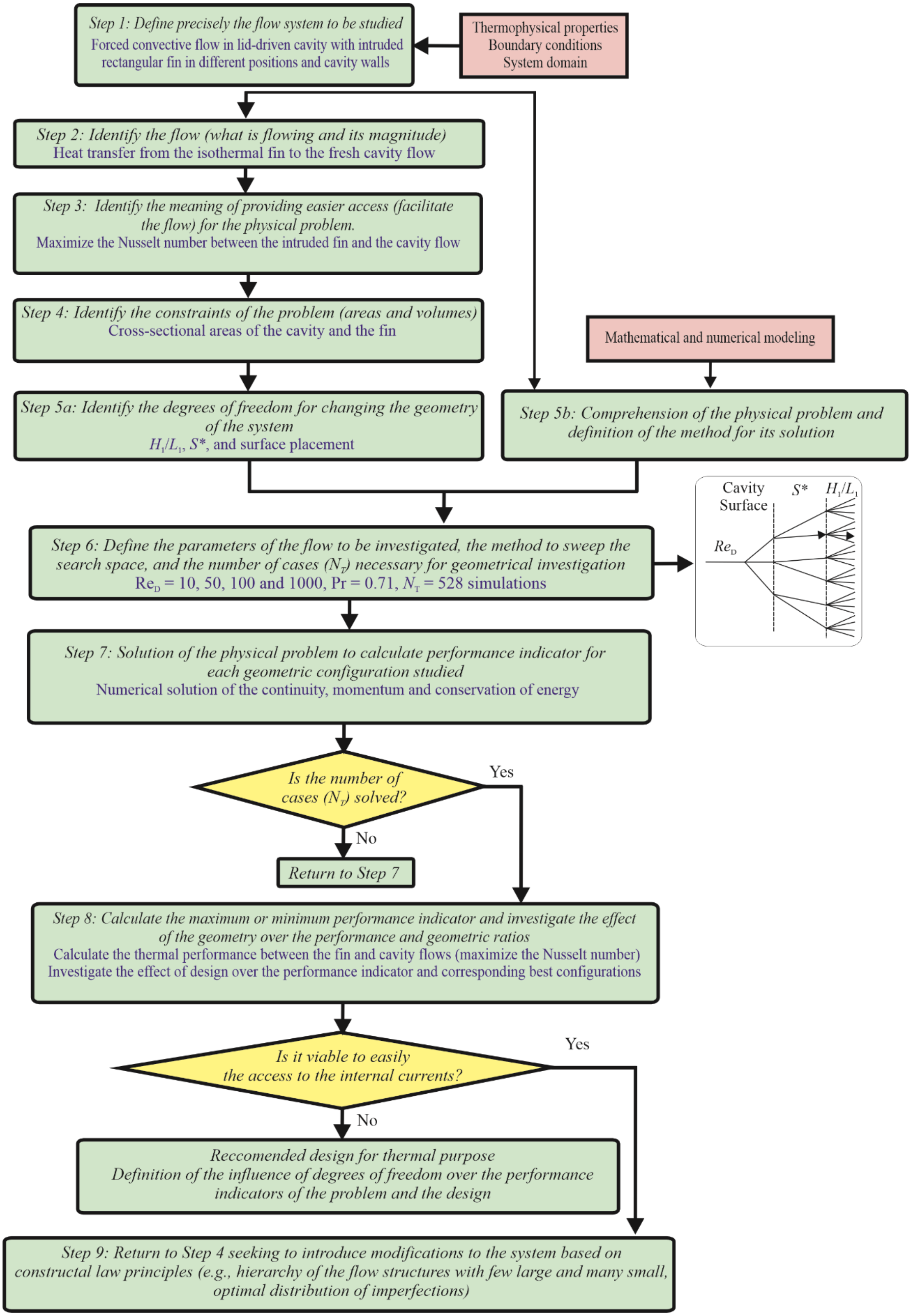

Fig 2: Flowchart for the present application of the Constructal Design method.

The ratio between the area filled by the fin and the cavity area can be determined as a dimensionless parameter by:

$$\phi = \frac{A_f}{A} \tag{10}$$

For the present study, it was assumed that ϕ = 0.05 for all cases. Furthermore, the height/length ratio of the cavity is considered constant as H/L = 1 to form a square cavity. Thus, in terms of the geometry of the problem, the aspect ratio of the height and length of the fin (H_1/L_1) is the degree of freedom that needs to be explored. The main objective is to identify the effect of H_1/L_1 on the Nusselt number for distinct Reynolds numbers $10 \leq Re_H \leq 1000$, and also placing the fin in five different positions (S^* = 0.1; 0.3; 0.5; 0.7; 0.9) on the low, downstream and the upstream surfaces of the cavity. The fin H_1/L_1 ratio was explored from 0.1 to 10.0, except for S^* = 0.1 and 0.9 where the minimal magnitude of H_1/L_1 = 2.0 is considered to avoid intersection between the fin and cavity surfaces. Fig. 3 summarizes the geometric evaluation process for the rectangular fin placed on the different sides of the cavity.

The heat transfer process in the problem was assessed using the Nusselt number, defined as dimensionless parameter that quantifies the relation of convection and conduction heat transfer mechanism [44]. It quantifies the heat transfer from the isothermal fin and the fluid flow, as specified by [44]:

$$Nu_H = \frac{h \cdot H}{k} = \frac{\partial T^*}{\partial n^*} \tag{11}$$

where n^* is the dimensionless coordinate in normal direction of the fin surface, h is the spatial averaged heat transfer coefficient, which can be used to calculate the heat transfer rate by Newton's cooling law:

$$q' = \frac{q}{W} = h p_{sf} \left(T_{\max} - T_{\min}\right) \tag{12}$$

where q is the heat transfer from the fin surface, p_{sf} is the perimeter of the fin, in all cases equal to $p_{sf} = (2H_1 + L_1)$, and W is the depth of the domain. Despite of the possibility to calculate the heat transfer rate, in this work it is focused on the geometries that conducted to heat transfer coefficient in the fin.

The geometric evaluation process was performed in four steps, as presented in Fig. 3. In the initial stage, the geometry of the fin was optimized by changing the ratio of H_1/L_1, while keeping the other degrees of freedom fixed (Re_H, cavity's surface, and fin position – S^*). Then, the highest Nusselt number is the once maximized Nusselt number ($Nu_{H,m}$), and the corresponding ratio H_1/L_1 is the once optimized ratio $(H_1/L_1)_o$. In the second step, the first step is repeated for different magnitudes of S^*, obtaining the twice maximized Nusselt number ($Nu_{H,mm}$), the twice optimized ratio $(H_1/L_1)_{oo}$ and the once optimized fin position $(S^*)_o$. In the third stage, the second step is repeated for the fin mounted in different cavity surfaces. Later, the first three steps are performed for various Re_H ($10 \leq Re_H \leq 1000$). All the investigations, varying the geometric configurations and Reynolds number led to a total of 528 simulated cases.

3. Numerical modeling and verification

The numerical solution of Eqs (1-4) was performed with the commercial computational fluid dynamics software Ansys Fluent (version 14), which is based on the Finite Volume Method [46 – 48]. The numerical scheme chosen to solve Eqs. (1) to (4) is based on the semi-implicit method for pressure linked equations (SIMPLEC). The first-order upwind interpolation method was chosen for the treatment of advective dominant flows. The solution was assumed to converge when at least two consecutive iterations are less than 10^{-6} for mass, 10^{-6} for momentum and 10^{-8} for the energy equation.

The numerical model and the mesh employed in this work are verified and validated from previous works of our research group [5, 40 – 43] in relation to other works in the literature. In this study, the velocity and temperature information simulated were compared to those found in the available literature for forced convective flow in a square lid-driven cavity with no fins on the surfaces. The results agree with the literature, suggesting that the numerical model and the mesh are adequate for this problem. Then, in this study, the mesh was generated using rectangular volumes and each mesh resulted in a total of nearly 40,000 volumes. For the sake of brevity, the verification and validation and the grid independence study are not repeated here, it can be seen in Refs. [5, 40 – 43].

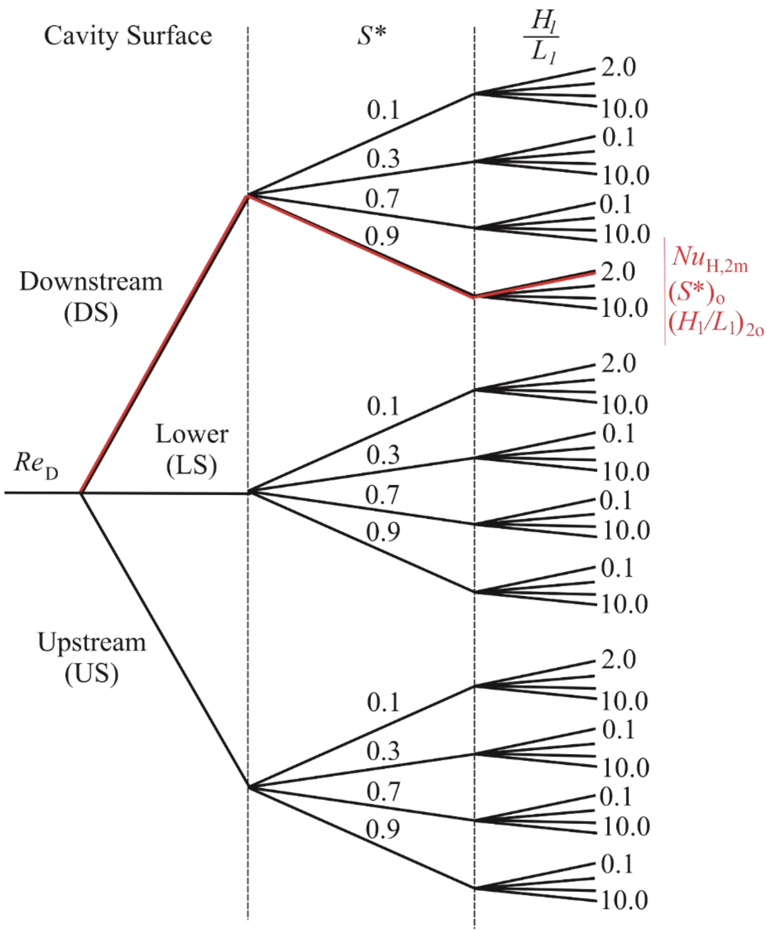

Fig 3: Schematic of the evaluation of geometric parameters surface (DS, LS or US), position (S*) and aspect ratio (H_1/L_1).

4. Results and discussion

4.1 Results for the fin at the low surface of the cavity

In this section, the temperature maps of several H_1/L_1 ratios were simulated to find the optimal fin shape that maximizes the average Nu_H. Initially, the fin was placed on the cavity's low surface. The variation of Reynolds numbers and the position of the fin (S^*) was investigated over Nu_H.

Fig. 4 presents the influence of the fin H_1/L_1 ratio on the Nu_H mounted on the low surface for S^* = 0.1 (a), S^* = 0.5 (b) and S^* = 0.9 (c) and for different Reynolds numbers. It is possible to observe that lower Reynolds numbers led to lower Nusselt numbers, while the highest Nusselt number was achieved for Re_H = 1000 for all cases. It demonstrates the tendency that the higher the flow intensity, the higher the Nu_H values, as expected. It is also worth noting that, for the case of Re_H = 10, the Nu_H number tends to demonstrate a small sensitivity with the H_1/L_1 ratio, while for higher Re_H, the difference between the highest and the lowest Nu_H numbers increases compared to the cases with lower Re_H.

In general, among the H_1/L_1 cases for S^* = 0.1 and 0.9 (Fig. 4 a and c), it can be seen that Nu_H values decrease when the H_1/L_1 ratio increases, except for Re_H = 10 where the lowest Nu_H was found for H_1/L_1 = 5.0. The lowest possible ratio $(H_1/L_1)_o$ = 2.0 is the one that leads to the highest Nu_H from the fin to the fluid flow for all Re_H evaluated. It is worth mentioning that even the Nu_H for S^* = 0.1 and S^*= 0.9 demonstrating similar trends, it could be different since the flow does not exhibit symmetrical tendencies because the incidence of the main vortex occurs differently for the two cases. On the other hand, when the fin was positioned at the center of the cavity's low surface (S^* = 0.5 - Fig. 4b), it was discovered that the best system performance is achieved with an intermediate H_1/L_1 ratio. This trend is similar when the fin is positioned in S^* = 0.3 and S^* = 0.7, so only the results for S^* = 0.5 are presented.

Fig. 5 presents the temperature maps for the maximum $Nu_{H,m}$ values achieved for the optimal $(H_1/L_1)_o$ ratios (left-hand temperature maps) in relation to the worst Nu_H values for different H_1/L_1 ratios (right-hand temperature maps) with different Re_H numbers and fixed S^* = 0.1. It is possible to observe a higher temperature in the left and lower regions of the cavity, especially between the fin and the upstream surface, which is the area where the fluid is trapped (stagnant). For the lowest Reynolds number (Re_H = 10) a more diffusive behavior was observed since the characteristics of the isotherms were more linear, and as the Reynolds number increases to Re_H = 100 and 1000, the main vortex has more intensity and the temperature gradients increase, especially in the region of the fins. For all cases, the increase in fin height resulted in a flow restriction and increased the temperature field, demonstrating that the highest H_1/L_1 ratios achieved the worst thermal performance. The optimal ratios $(H_1/L_1)_o$, usually with lower heights, improved the Nu_H numbers about 11.7, 20.3 and 20.6% in relation to the worst cases observed for Re_H = 10, 100 and 1000, respectively. In general, the increase in the heat exchange surface area is not a sufficient condition to maximize Nu_H in an internal flow convection problem if there is a restriction of the fluid flow.

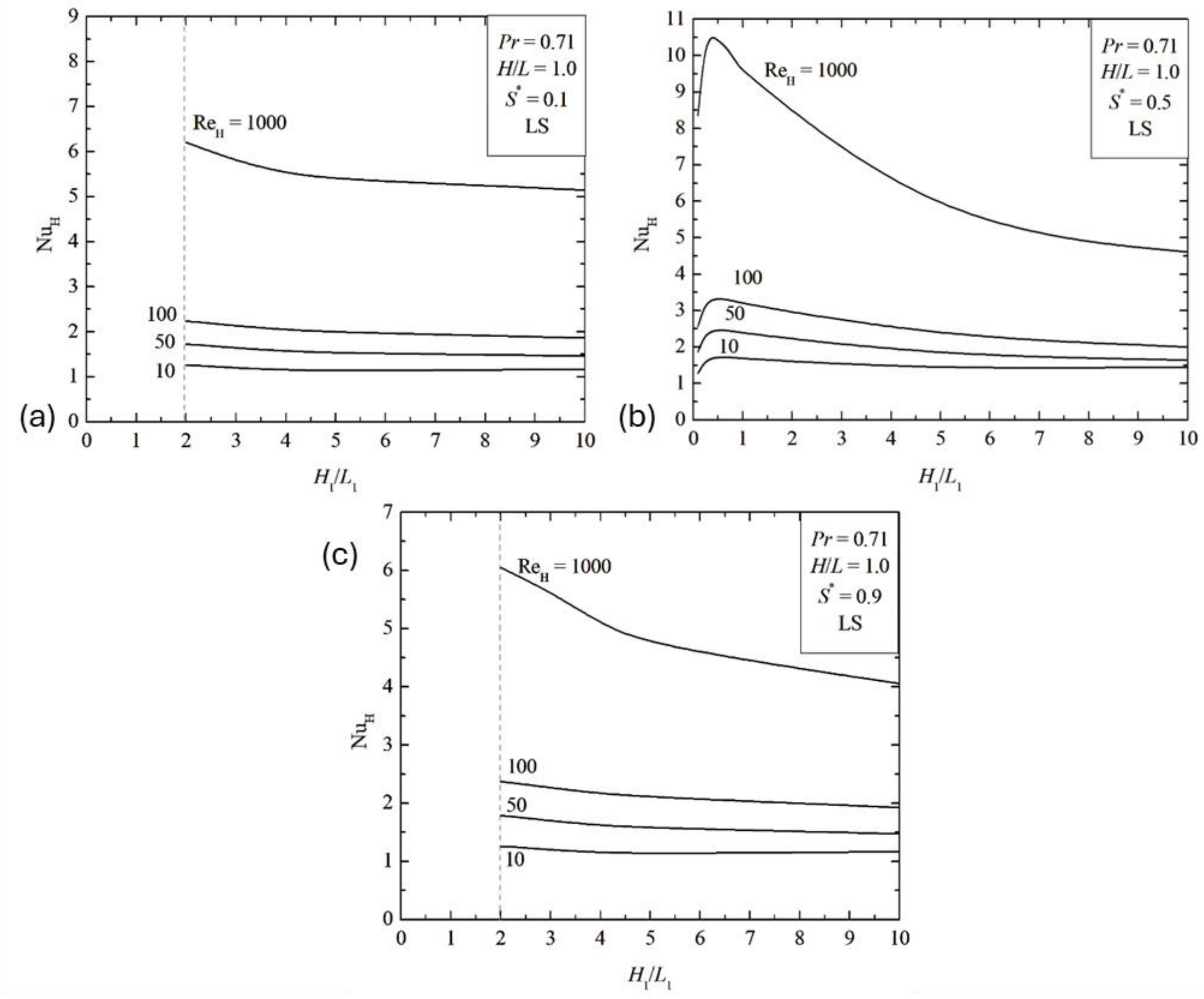

Fig. 4 – Effect of the ratio H_1/L_1 over Nu_H in LS position for Re_H and S^*: a) S^* = 0.1, b) S^* = 0.5, c) S^* = 0.9.

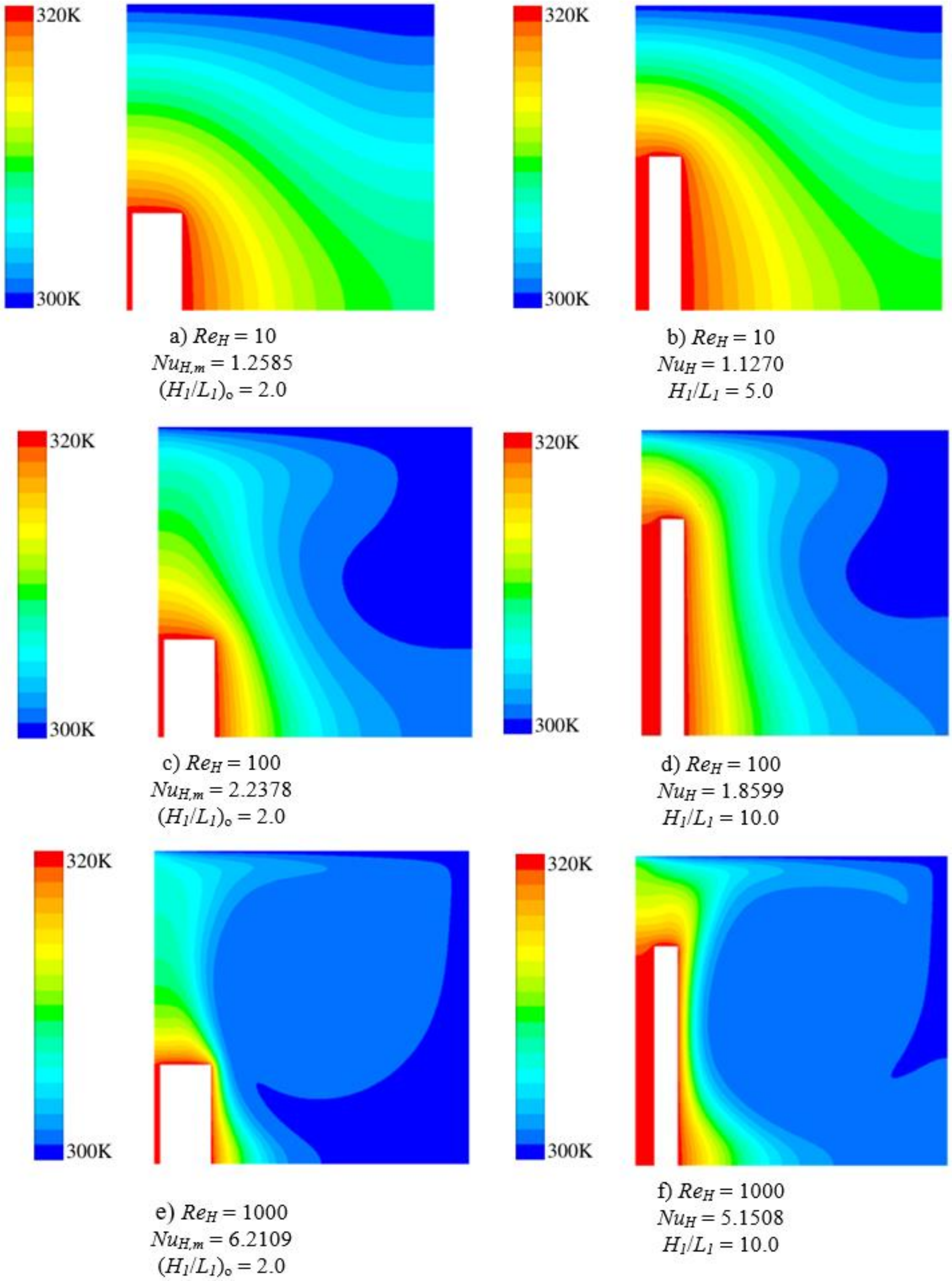

Fig. 5 – Temperature maps for some best and worst configurations for a rectangular fin placed on the low surface and $S^* = 0.1$.

The temperature maps obtained by the rectangular fin positioned in the middle of the low surface of the cavity ($S^* = 0.5$) are illustrated in Fig 6. This figure presents the maximized $Nu_{H,m}$ values achieved by the optimal $(H_1/L_1)_o$ ratios in the left-hand side (Figs. 6 a, c and e) and the worst Nu_H values by different H_1/L_1 in the right-hand side (Figs. 6 b, d and f) in relation to different Reynolds numbers. The temperature map is not so affected when Re_H = 10. For this case, the fluid flow has a low intensity, and the isothermals are almost linear. Therefore, the fluid flow is restricted to the upper downstream corner of the cavity. As a result, the temperature map are slightly different for the optimal $(H_1/L_1)_o$ ratio in relation to the worst case. Nevertheless, the $(H_1/L_1)_o$ ratio increased the Nu_H by about 34.0% in relation to the worst H_1/L_1 ratio. However, the differences in the temperature map for the best and worst H_1/L_1 ratios rise as the Re_H increases, as shown in Figs. 6 (c, d, e, and f). As the Re_H increases, the intensity of the main vortex increases, reaching the lower regions of the cavity and enhancing the heat transfer through the fin. It is worth noting that higher H_1/L_1 ratios were the worst cases, as it suppresses the main vortex in the top area of the cavity, increasing the temperature in the lower and left side regions of the cavity (Fig. 6d, f). It is more evident for the case Re_H = 1000, where the primary vortex penetrates even more into the cavity, meagering the heat exchange in the lower cavity regions for the H_1/L_1 = 10. The difference in the Nu_H between the optimal and worst H_1/L_1 ratios was 65.2 and 128.5% for Re_H = 100 and 1000, respectively.

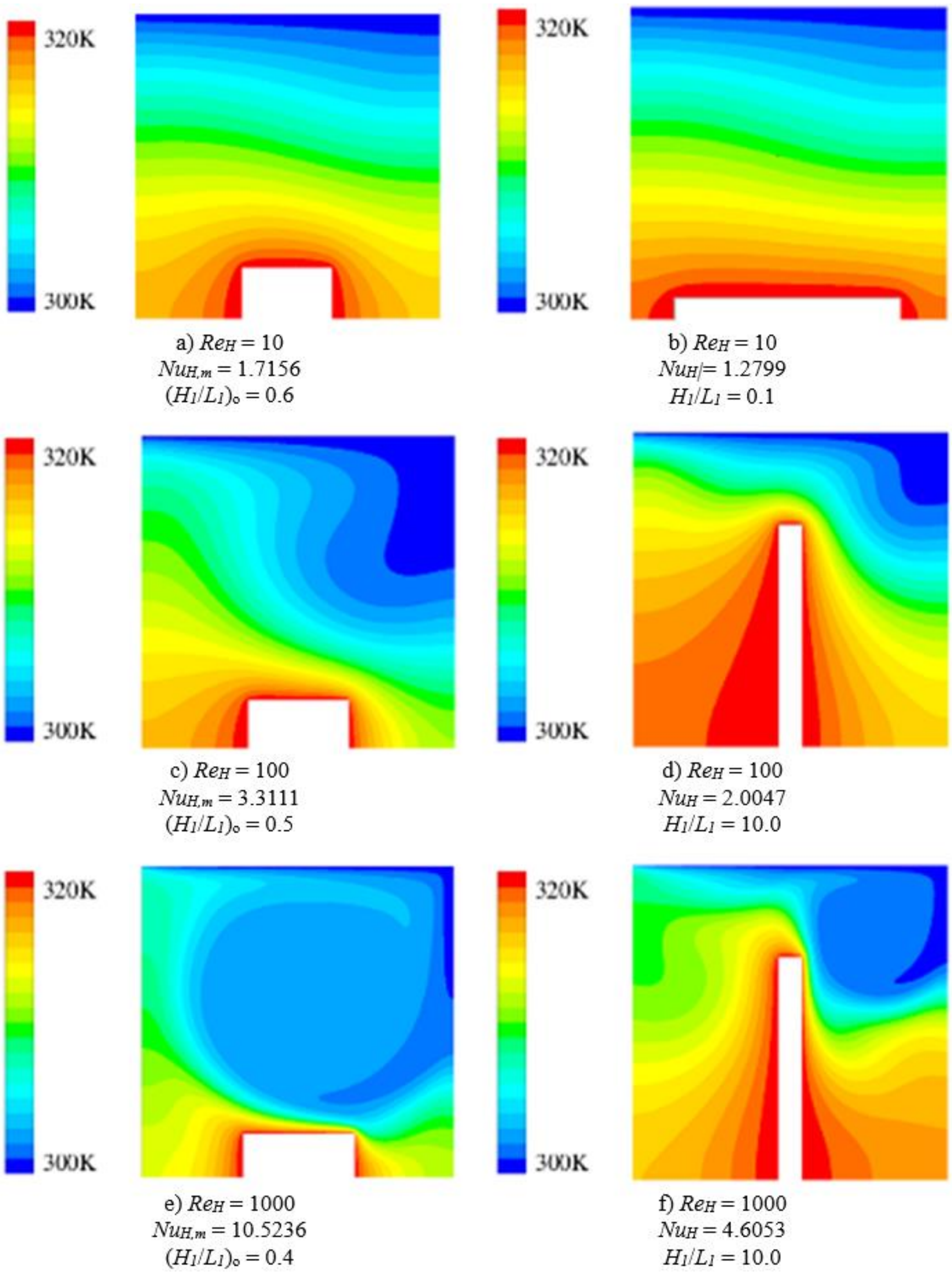

Fig. 6 – Temperature maps for some best and worst configurations for a rectangular fin placed on the low surface and S^* = 0.5.

Fig. 7 illustrates the temperature maps for the optimal and the worst cases geometries for flows with Re_H = 10, 100 and 1000 and S^* = 0.9. In general, like the previous case (S^* = 0.1), the main vortex is suppressed when the fin has a greater penetration in the *y*-direction of the cavity. It can also be seen that, unlike in the case of S^* = 0.5, the main vortex cannot propagate in the area between the fin and the downstream surface of the cavity in cases with a higher H_1/L_1 ratio. This slightly change the distribution of temperature fields throughout the cavity. The $(H_1/L_1)_o$ = 2.0 ratio was the best fin shape for these cases while the worst one was H_1/L_1 = 5.0 for Re_H = 10, and H_1/L_1 = 10.0 for Re_H = 100 and 1000. The $(H_1/L_1)_o$ improved the Nu_H number about 11.8, 23.5 and 49.2% in relation to the Nu_H for the worst H_1/L_1 ratios.

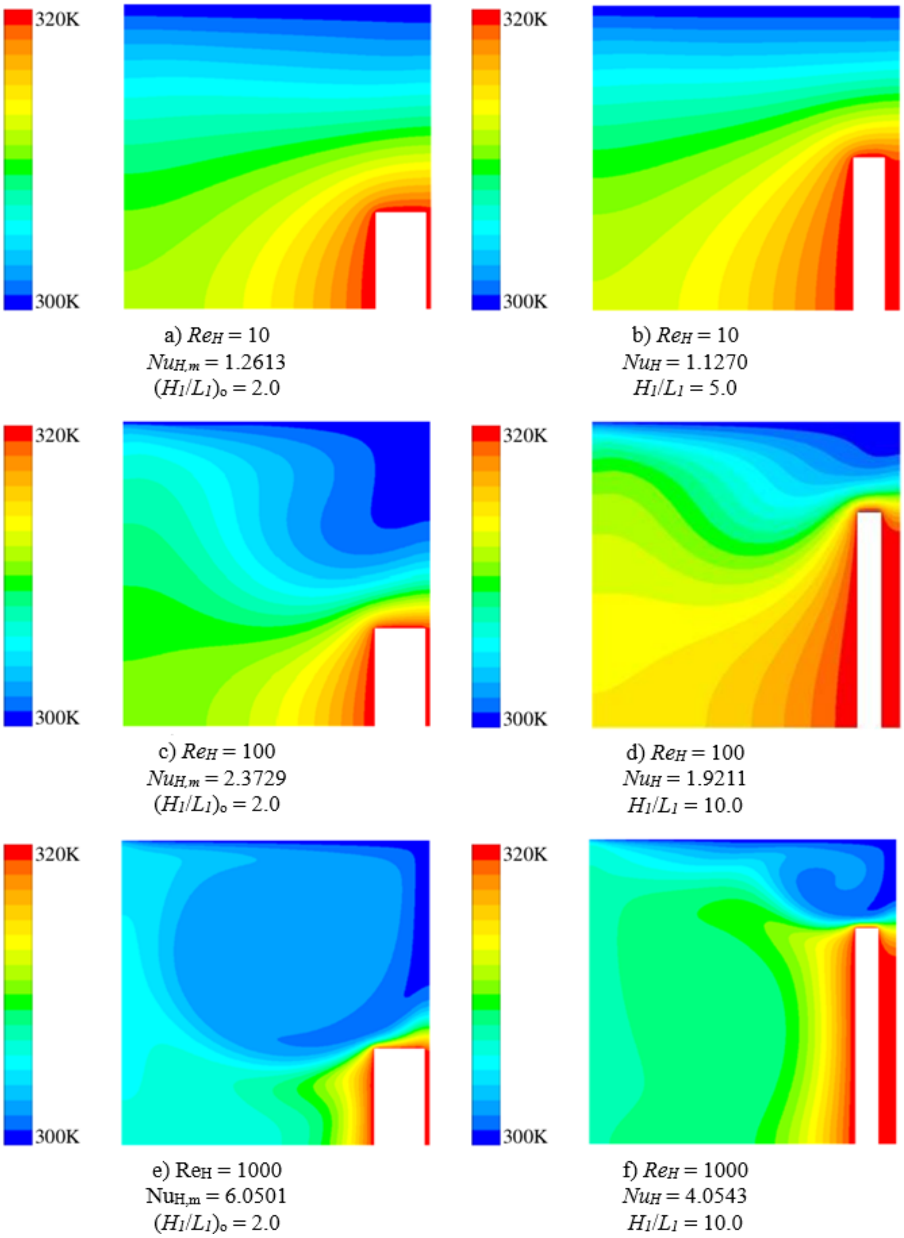

Fig. 7 – Temperature maps for some best and worst configurations for a rectangular fin placed on the low surface and S^* = 0.9.

All the maximized $Nu_{H,m}$ numbers and optimum $(H_1/L_1)_o$ ratios results achieved for the rectangular fin placed in the low surface of the cavity can be compiled and ploted in relation to the distance S^*, as shown in Fig. 8 (a) and (b), respectively. Fig. 8a illustrates that the Nu_H is lower when the fin is positioned at the beginning or end of the cavity - lower and higher values of S^* - for all Re_H. Conversely, the highest $Nu_{H,m}$ values were achieved when the fin was positioned more in the middle of the cavity for all Re_H values. As previously mentioned, when the fin is positioned at the beginning or end of the cavity, part of the flow is trapped (stagnated) between the lateral of the fin and the cavity, which decreases the heat transfer and the Nusselt number. Otherwise, once the fin was positioned in the middle of the cavity (S^*=0.5), it facilitated the main vortex to remove heat from the entire fin surface, increasing the system's thermal performance. In the highest Re_H number case (Re_H = 1000), the optimal geometry obtained was for $(S^*)_o$ = 0.5 and $(H_1/L_1)_{oo}$ = 0.4, which led to a twice-maximized Nusselt number of $Nu_{H,mm}$ = 10.5236.

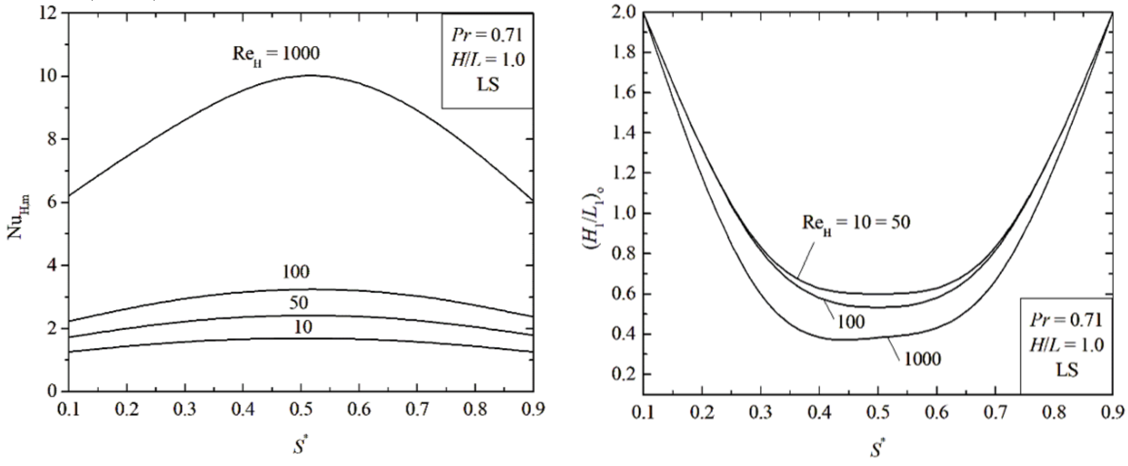

a) b)

Fig. 8 – Effect of distance S^* for a rectangular fin placed at the low surface on: a) the once maximized Nusselt number, $Nu_{H,m}$, b) once optimized ratio H_1/L_1, $(H_1/L_1)_o$.

Fig. 8b presents the impact of the position of the fin (S^*) over the optimized $(H_1/L_1)_o$ ratio. At the ends of the cavity, the values are higher, and it decreases for intermediate values of S^*. It is also worth mentioning that in the range $10 \leq Re_H \leq 100$, the behaviour of $(H_1/L_1)_o$ is symmetrical, i.e. the optimal geometries obtained for S^* = 0.1 and 0.9 are equal to $(H_1/L_1)_o$ = 2.0 and for S^*= 0.3 and 0.7 they are also around $(H_1/L_1)_o \sim 0.8$. However, for Re_H = 1000, this behaviour is no longer symmetric. It can be attributed to the fact that the primary vortex is more intense, and the incidence of this vortex is different for $S^* < 0.5$ and $S^* > 0.5$. Thus, the optimal geometry is a consequence of the flow asymmetry, where the primary vortex goes from the top right corner to the middle of the cavity.

4.2 Results for the fin at the downstream surface of the cavity

Fig. 9 presents the effect of H_1/L_1 over the Nu_H for the fin placed on the positions of S^* = 0.1 (a), 0.5 (b) and 0.9 (c) on the downstream surface of the cavity. The Nu_H increases as the Re_H increases for all cases. The results indicated that the optimal geometry found was $(H_1/L_1)_o$ = 2.0 for all Re_H when the fin was placed in S^* = 0.1 (a) and S^* = 0.9 (c). However, it is evident from Fig. 9a that Nu_H smoothly increases when H_1/L_1 decreases for the S^* = 0.1. However, Nu_H sharply increases when H_1/L_1 decreases for the S^* = 0.9, Fig. 9c, especially for H_1/L_1 ratios lower than 4.0, reaching a maximum value of Nu_H = 28.55 for $(H_1/L_1)_o$ = 2.0. This difference may be attributed to the fin being positioned near to the top surface of the cavity for S^* = 0.9. Then, the Nu_H is more sensitive to fluid flow and the heat transfer compared to the fin positioned at S^* = 0.1. It is also apparent from Fig. 9c that the Nu_H results for Re_H between 10 and 100 are very close to each other, indicating that there are no significant improvements to increase Re_H since the heat transferred is almost the same for these cases. From Fig. 9b, it is possible to observe a similar trend when the fin is positioned on S^* = 0.5 at the low surface (Fig. 4b). However, when the fin is positioned at the middle of the downstream surface, the Nu_H values are a bit higher than the ones found in Fig. 4b. It is also noted that the optimal $(H_1/L_1)_o$ ratios are not equal to Fig. 9a and 9b. In these cases, it was found that the optimum fin shape that led to the best heat transfer performance were low and intermediate H_1/L_1 ratios.

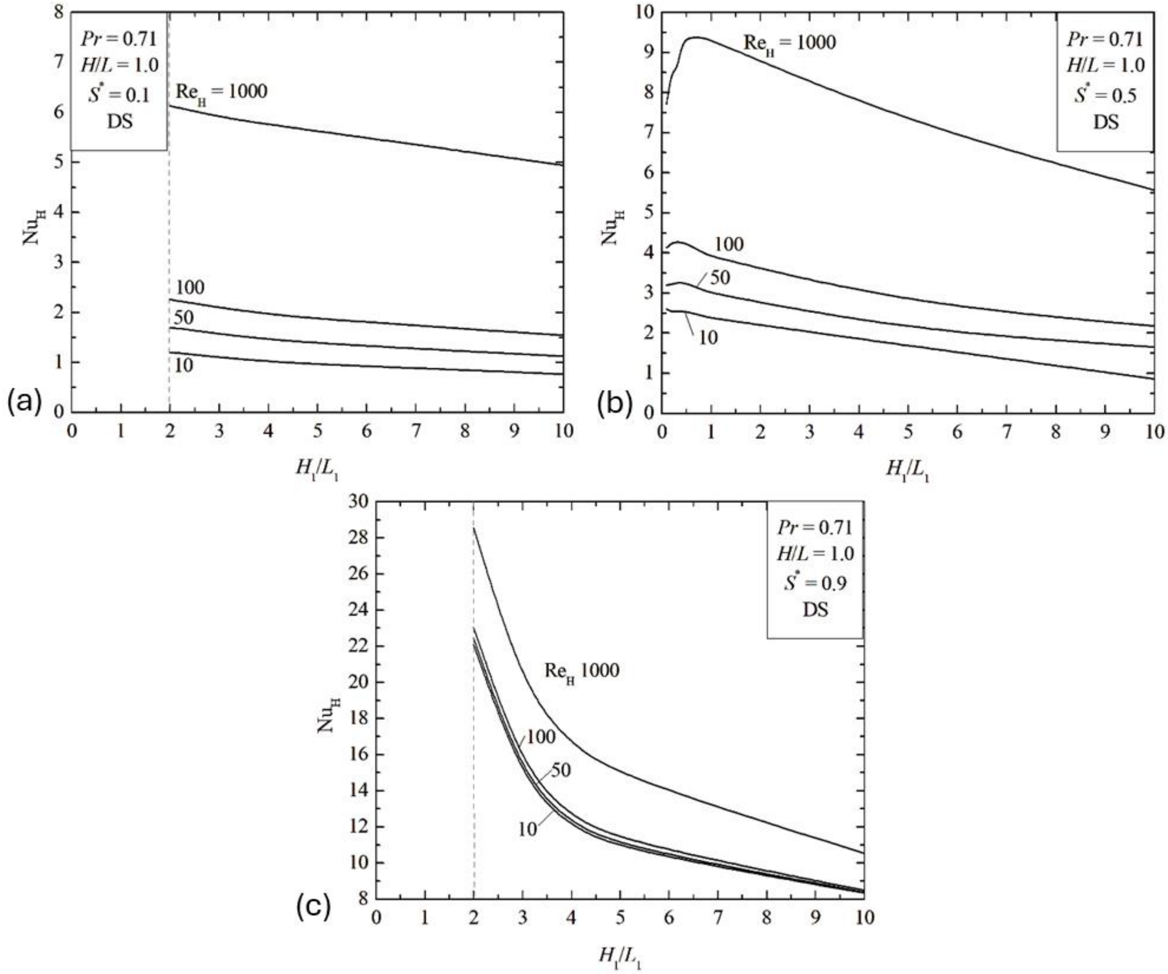

Fig. 9 - Effect of the ratio H_1/L_1 over Nu_H for the rectangular fin mounted on the downstream surface of the cavity considering different Re_H and S^*: a) $S^* = 0.1$, b) $S^* = 0.5$, c) $S^* = 0.9$.

The temperature maps for the rectangular fin placed on the downstream surface of the cavity at the position $S^* = 0.1$ in relation to Re_H are shown in Fig. 10. The Figs. 10a, 10c and 10e illustrate the temperature maps for the optimal $(H_1/L_1)_o$ ratios and the maximized $Nu_{H,m}$ while the Figs. 10b, 10d and 10f present the temperature maps for the worst H_1/L_1 ratios cases. In general, it can be seen that the fins with optimal geometries, lower $(H_1/L_1)_o$ ratios, do not significantly affect the flow of the main vortex, leading to higher temperature gradients on the top and left side of the fin surfaces. On the other hand, when the fin geometry has a high H_1/L_1 ratio, the main flow is trapped in the upper region of the fin, restricting the fluid flow, and decreasing the Nu_H. These results trends become more evident in the temperature maps for higher Re_H when the fluid flow has a higher intensity. The optimal fin geometries enhanced the Nu_H about 25.5, 46.5 and 24.0% compared to the worst fin geometries for Re_H of 10, 100 and 1000, respectively.

Fig. 11 shows the temperature maps for the best and worst fin geometries when the fin is positioned at the center of the downstream surface of the cavity ($S^* = 0.5$) for Re_H from 10 to 1000. Figs. 11a, 11c, and 11e present the maximized $\mathrm{Nu}_{H,m}$ for $(H_1/L_1)_o$, while the Figs. 11b, 11d and 11f present the lowest values of Nu_H for the worst H_1/L_1 ratios tested. The optimal fin geometry is not the same for all cases; it varies from $(H_1/L_1)_o = 0.1$, 0.3 and 0.7 for $Re_H = 10$, 100 and 1000, respectively. This can be attributed to modifications in the fluid flow and the thermal behavior. For $Re_H = 10$, the optimal fin geometry has a large left-side edge, so the heat was mainly removed on this side. However, when the Re_H increased to 1000, the optimal fin geometry $(H_1/L_1)_o = 0.7$ has more uniform surfaces and the heat was removed in more homogeneous way. Furthermore, once the fin H_1/L_1 ratios increase, it restricts the fluid flow and heat transfer in the lower region of the cavity, trapping part of the flow in the top area of the cavity. As a result, heat transfer from the fin to the surrounding flow is limited in the cavity's low surface. For all cases, the worst fin geometry found was the $H_1/L_1 = 10.0$. The optimal fin geometries found for $S^* = 0.5$ represented a difference of 66.8, 48.9 and 40.0 % in relation to the H_1/L_1 = 10.0 ratio.

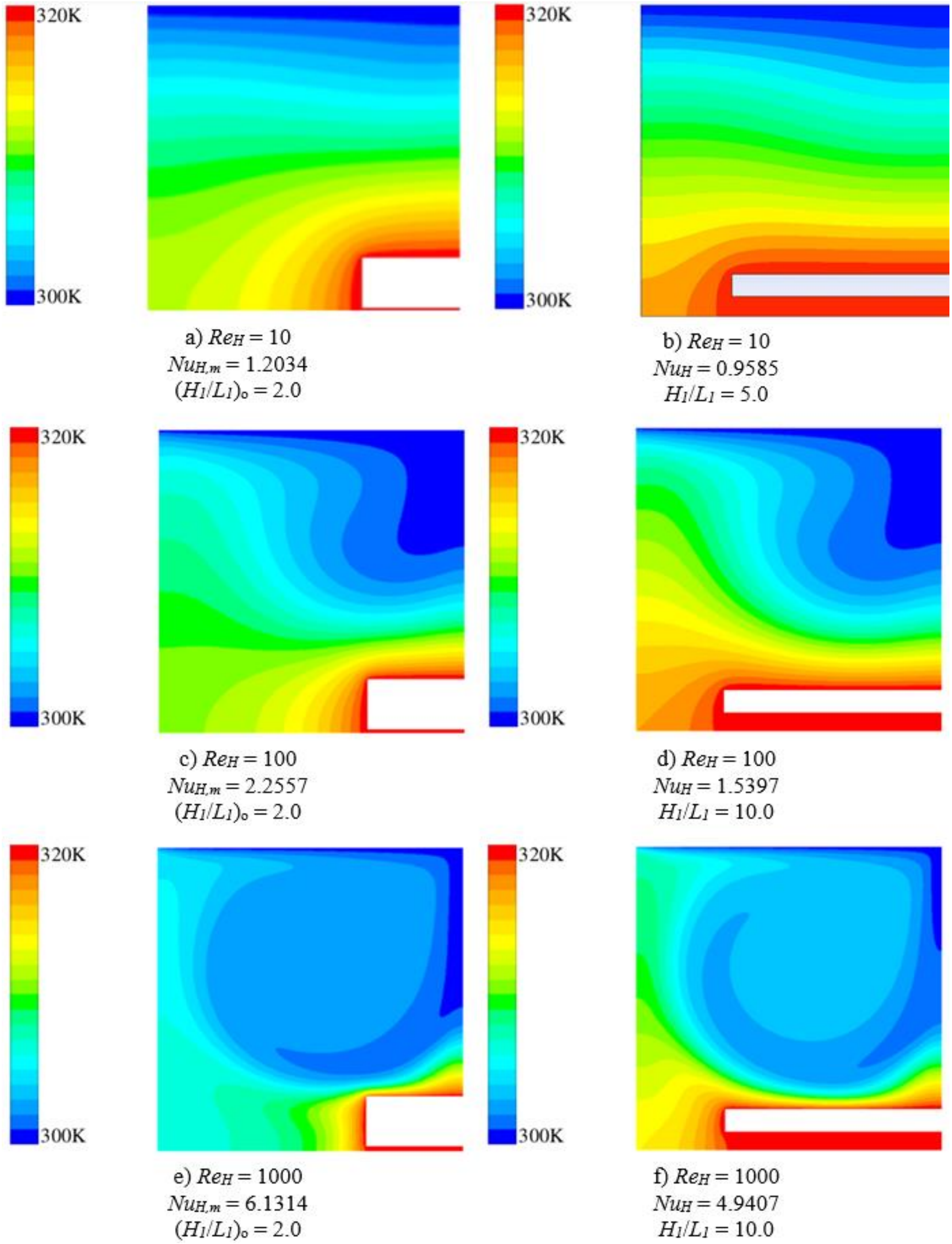

Fig. 10 – Temperature maps for some best and worst configurations for a rectangular fin placed on the downstream surface and S^* = 0.1.

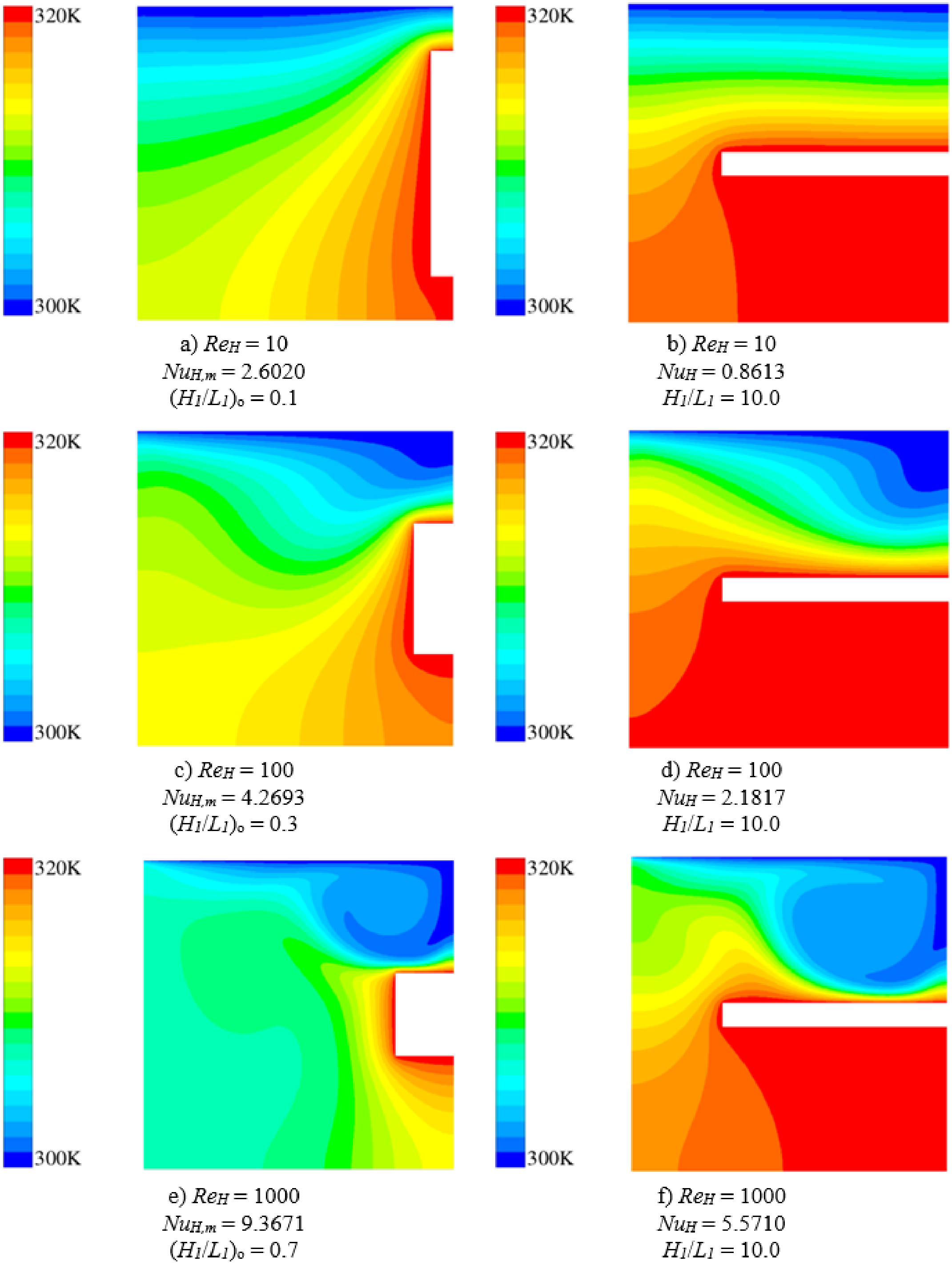

Fig. 11 – Temperature maps for some best and worst configurations for a rectangular fin placed on the downstream surface and $S^* = 0.5$.

Fig. 12 shows the temperature maps for the optimal ratios (Fig. 12 a, c, e) and the cases with the worst geometries (Fig. 12 b, d, f) in relation to Re_H for the fin positioned at $S^* = 0.9$ at the downstream surface of the cavity. In these cases, the temperature fields are significantly influenced by the top surface of the fin, causing an increase in the temperature gradients in the gap between the fin and the top surface of the cavity. It is worth noting that this condition is only possible due to the imposition of the flow in the lid-driven surface. For all cases, the

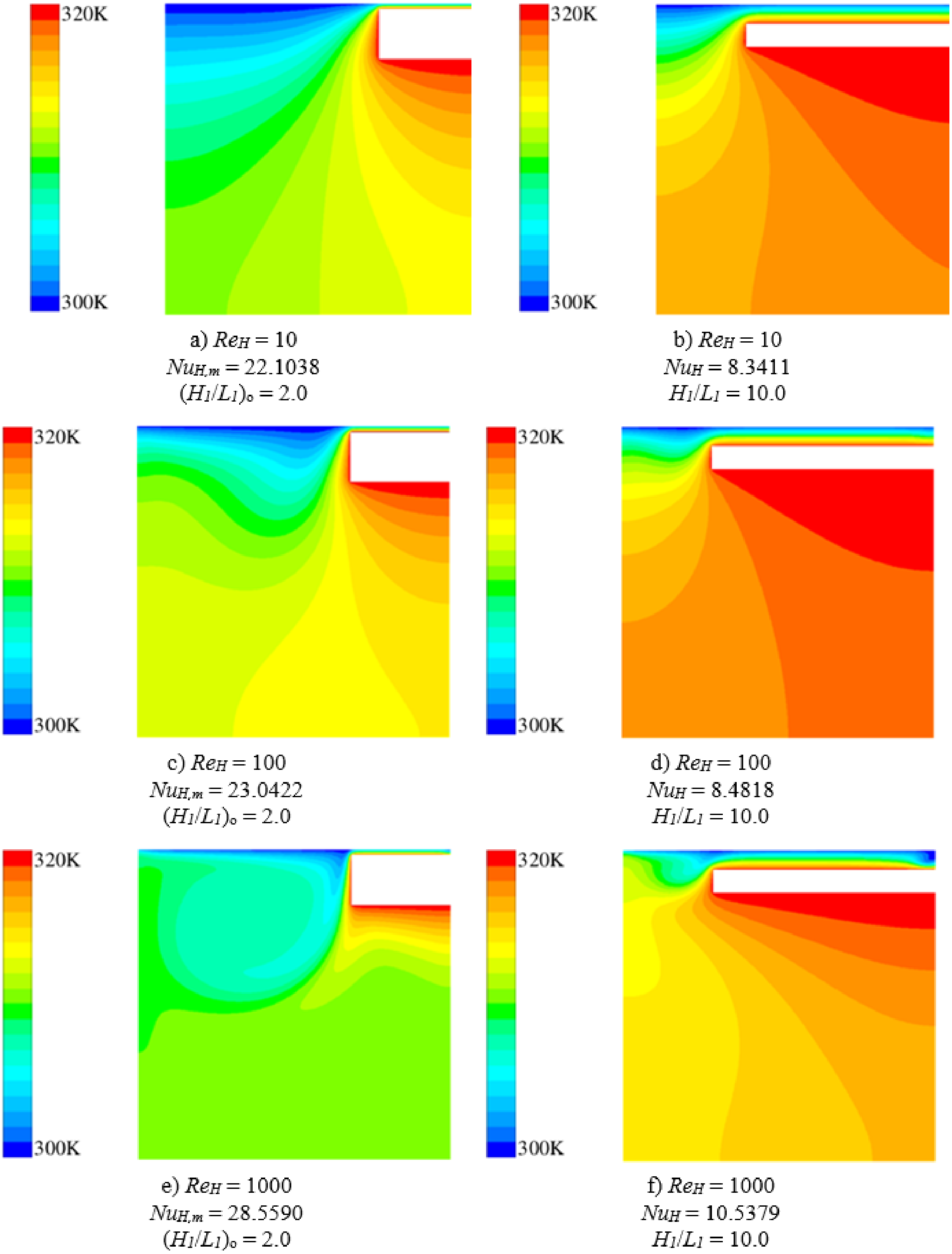

Fig. 12 – Temperature maps for some best and worst configurations for a rectangular fin placed on the downstream surface and $S^* = 0.9$.

optimal $(H_1/L_1)_o$ ratios were 2.0, which generated the narrowest gap possible between the fin and cavity for the studied cases, while the worst cases were $H_1/L_1 = 10.0$. For $Re_H = 1000$, the maximized $Nu_{H,m}$ was 28.5590, which was significantly higher than the worst case with $Nu_H = 10.537$ for $H_1/L_1 = 10.0$. As mentioned above, for higher H_1/L_1 ratios, the fluid flow is restricted to the top region of the cavity, making it difficult to remove heat from the bottom of the fin. However, for lower H_1/L_1 ratios, the fluid flow has more access to the bottom and side walls of the fin, improving the heat transfer and increasing Nu_H. It is also possible to note that the Nu_H are similar for the cases with lower Re_H. It was achieved $Nu_{H,m}$ = 22.1038 and 23.0422 for Re_H = 10 and 100 with $(H_1/L_1)_o$ = 2.0, respectively. It might be attributed to the similar formation of the main vortex for these cases. Then, the magnitudes of Nu_H are very similar for Re_H in the range $10 \leq Re_H \leq 100$.

Results from the rectangular fin positioned on the downstream surface of the cavity are summarized in Fig. 13 that show the influence of the distance S^* on the once maximized Nusselt number (a) and the once optimized ratio $(H_1/L_1)_o$ (b). Fig. 13a shows that the twice maximized $Nu_{H,mm}$ was obtained once the fin was close to the top surface of the cavity for $(S^*)_o$ = 0.9. The results also show a considerable decrease in the Nu_H values as S^* decreases. For example, for Re_H = 1000, the optimal geometry with $(H_1/L_1)_{oo}$ = 2.0 and $(S^*)_o$ = 0.9 leads to a twice maximized $Nu_{H,mm}$ = 28.5591, which is 4.66 times higher than the worst once optimized $Nu_{H,m}$ for the same Re_H number with S^* = 0.1 and $(H_1/L_1)_o$ = 2.0. Fig. 13b shows that the highest optimal $(H_1/L_1)_o$ ratio was 2.0 when the fin is positioned at the extremes of downstream surface of the cavity. As previously shown in the temperature maps, it justifies because for higher H_1/L_1 ratios, the main vortex ends up being suppressed in the top section of the cavity, decreasing the heat transfer on the left and lower region of fin surface. For intermediate ratios of S^*, the magnitudes of $(H_1/L_1)_o$ decreased even more, with different magnitudes depending on the Re_H.

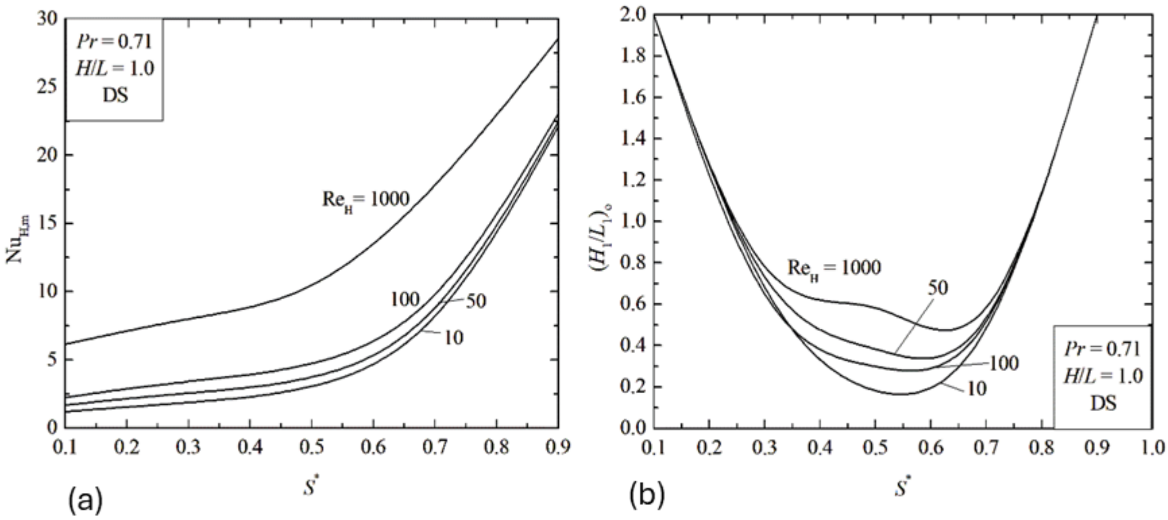

Fig. 13 – Effect of distance S^* for a rectangular fin placed at the downstream surface on: a) the once maximized Nusselt number, $Nu_{H,m}$, b) once optimized ratio H_1/L_1, $(H_1/L_1)_o$.

4.3 Results for the fin at the upstream surface of the cavity

Finally, the Nu_H in relation to the H_1/L_1 ratios for the rectangular fin placed on the upstream surface of the cavity surface in the positions S^* = 0.1 (a), 0.5 (b) and 0.9 (c) for different Re_H are shown in Fig. 14. These results are like the ones achieved for the fin positioned on the downstream surface of the cavity. It was noted a decrease in Nu_H when H_1/L_1 increases for S^* = 0.1 and 0.9. Therefore, lower H_1/L_1 ratios led to the highest Nu_H values for these cases. Once the fin was positioned near the cavity's lower surface (S^* = 0.1), there was a slight difference in the fin geometries over the Nu_H. However, when the fin is positioned close to the upper region of the cavity (close to the imposed fluid flow), it is possible to observe higher Nu_H values depending on the H_1/L_1 ratio. It can also be seen in Fig. 14b that for S^* = 0.5, there was an intermediate optimal $(H_1/L_1)_o$ ratio for all Re_H investigated. In addition, the highest H_1/L_1 ratios lead to the worst Nu_H.

Fig. 15 presents the temperature maps for fin placed on the upstream surface of cavity and S^* = 0.1 for the maximized $Nu_{H,m}$ and the worst cases. For the same S^* = 0.1, the findings show a similar trend for the fin positioned on the cavity's downstream surface. Regarding the temperature maps, it slightly differs from the case of the fin on the downstream surface of the cavity. However, there are no significant differences from the temperature gradient close to the fin since it was positioned close to the lower surface of the cavity.

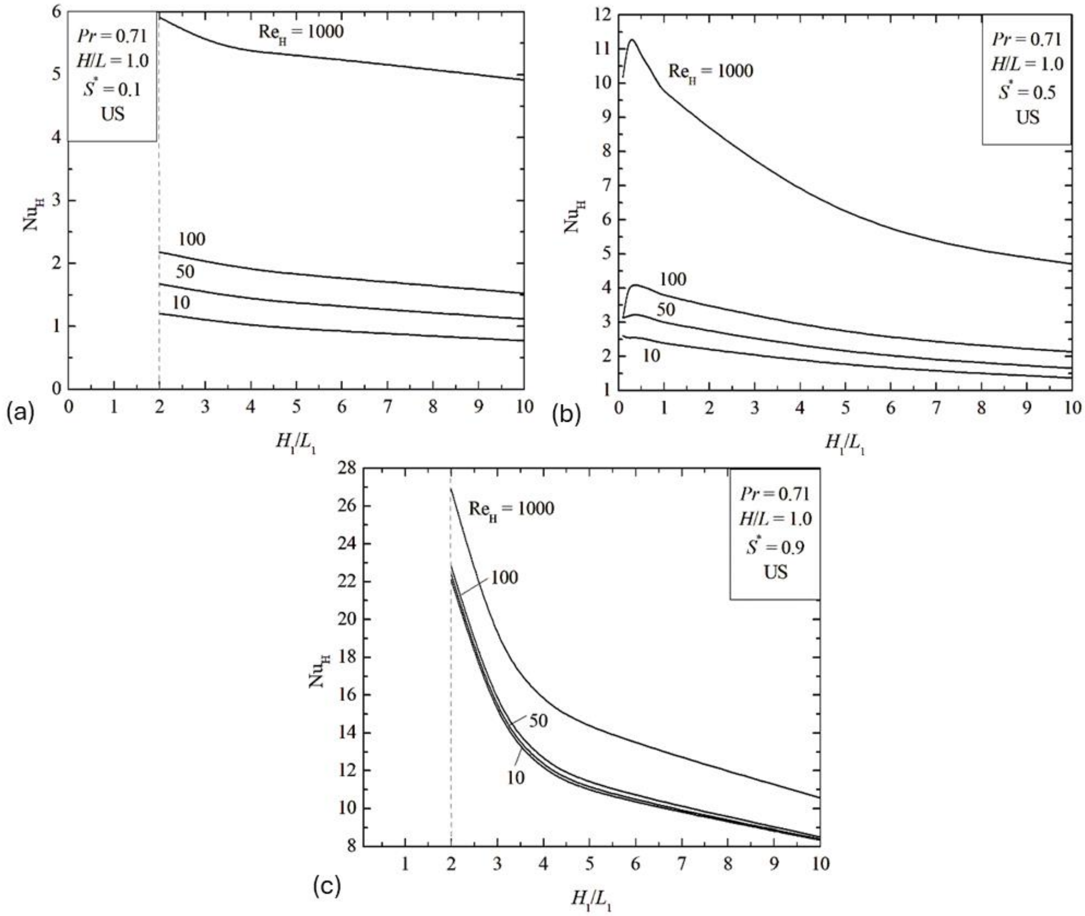

Fig. 14 – Effect of the ratio H_1/L_1 over Nu_H for the rectangular fin mounted in upstream surface of the cavity considering different Re_H and S^*: a) $S^* = 0.1$, b) $S^* = 0.5$, c) $S^* = 0.9$.

Fig. 16 presents the temperature maps for the optimal $(H_1/L_1)_o$ ratios (Fig. 16 a, c, e) and the cases with the worst geometries (Fig. 16 b, d, f) in relation to Re_H for the fin positioned at $S^* = 0.9$ on the cavity's upstream surface. For the worst fin H_1/L_1 ratios, the fin restricts the primary vortex in the top region of the cavity, similar to what was observed with the increase in S^* when the fin is placed in the DS cavity position. For the $(H_1/L_1)_o$ the fluid flow is not trapped in the upper region of the cavity, enhancing the $Nu_{H,m}$ and achieving the maximum value of $Nu_{H,m}$ = 11.3283 for Re_H = 1000. It is worth mentioning that the optimal $(H_1/L_1)_o$ ratios are not the same as the one found for S^* = 0.5 when the fin is placed at the downstream surface. It occurs because the flow is asymmetric since the main vortex is formed in the top right corner and moves towards the center of the cavity, causing the flow incidence to be different from one fin to another. This is not noticeable for the case with Re_H = 10 as the flow intensity is low.

The temperature maps reached for the optimal and worst fin configurations for the rectangular fin placed on the upstream surface of cavity and S^* = 0.9 are shown in Fig. 17. The optimal $(H_1/L_1)_o$ = 2.0 and the worst H_1/L_1 =10.0 found are the same of the ones found when the fin is positioned in the downstream surface of the cavity for S^* = 0.9. However, the temperature maps are not the same since the fluid flow is non-asymmetrical. In particular, for the optimal case with Re_H = 1000, the temperature maps are different from Fig. 17e and Fig. 12e, and it can be attributed to the difference of how the main vortex is generated and how it goes to the lower region of the cavity. For the fin positioned on the upstream surface, the main vortex flows on the lower surface of the fin. However, in the case of the fin positioned on the downstream surface of the cavity, the main vortex is generated on the left side of the fin, making it harder to go to the lower surface of the fin, affecting the temperature map.

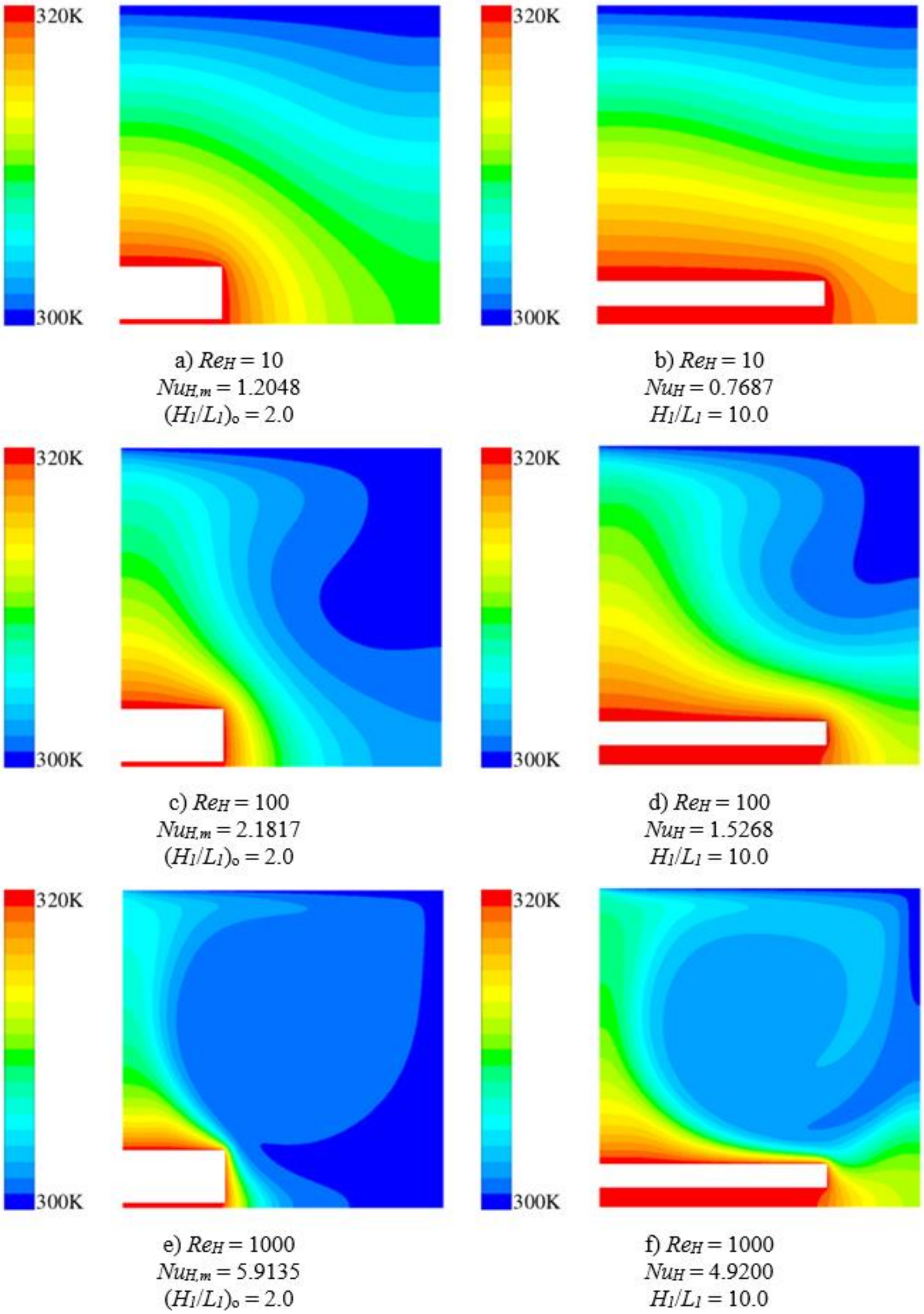

Fig. 15 – Temperature maps for some best and worst configurations for a rectangular fin placed on the upstream surface and $S^* = 0.1$.

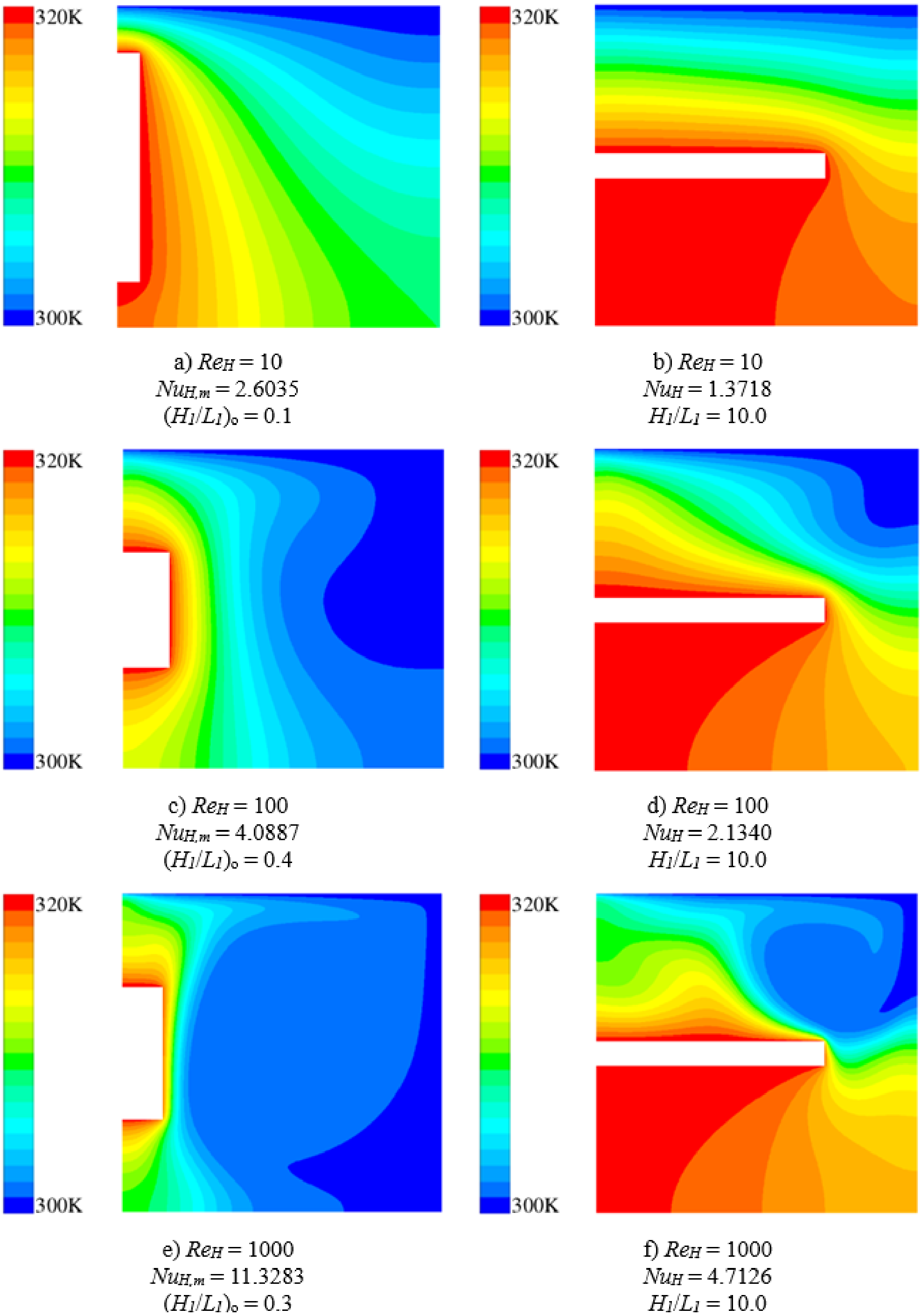

Fig. 16 – Temperature maps for some best and worst configurations for a rectangular fin placed on the upstream surface and $S^* = 0.5$.

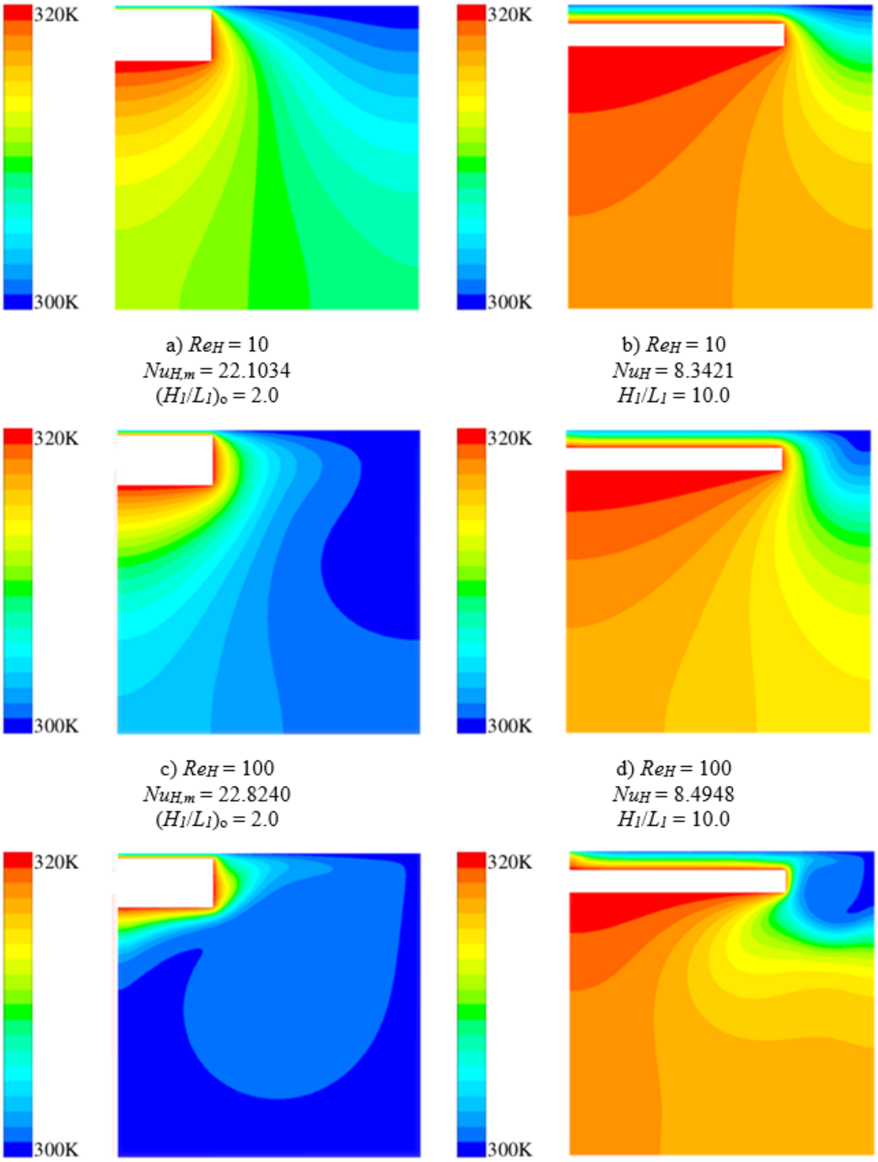

a) $Re_H = 10$
$Nu_{H,m} = 22.1034$
$(H_1/L_1)_o = 2.0$

b) $Re_H = 10$
$Nu_H = 8.3421$
$H_1/L_1 = 10.0$

c) $Re_H = 100$
$Nu_{H,m} = 22.8240$
$(H_1/L_1)_o = 2.0$

d) $Re_H = 100$
$Nu_H = 8.4948$
$H_1/L_1 = 10.0$

e) $Re_H = 1000$
$Nu_{H,m} = 26.8870$
$(H_1/L_1)_o = 2.0$

f) $Re_H = 1000$
$Nu_H = 10.5596$
$H_1/L_1 = 10.0$

Fig. 17 – Temperature maps for some best and worst configurations for a rectangular fin placed on the upstream surface and $S^* = 0.9$.

Fig. 18 shows the effect of the S^* on the $Nu_{H,m}$ (a) and the effect of the S^* on the optimized $(H_1/L_1)_o$ values (b) in relation to Reynolds. The best $Nu_{H,m}$ results were obtained for $S^* = 0.9$. In general, the results trends were similar to the case of the fin inserted in the downstream surface of the cavity. It is interesting to note that for the same Re_H = 1000, the optimized fin geometry was $(H_1/L_1)_{oo} = 2.0$ and $S^* = 0.9$ achieved a $(Nu_{H,m}) = 26.8870$, which is 4.55 times higher than the case of once optimized $(H_1/L_1)_o = 2.0$ and $S^* = 0.1$, where $Nu_H = 5.913478$. Regarding the optimized $(H_1/L_1)_o$ as a function of S^* (Fig. 18b), it is possible to note that they are similar to those for the fin mounted in the downstream surface of the cavity. The optimal $(H_1/L_1)_o$ ratio was 2.0 for the fin positioned in the extremes of the upstream surface. It is explained by the fact that H_1/L_1 ratios greater than 2.0 suppress the main vortex at the top area of the cavity, decreasing the heat transfer on the bottom of the fin surface. It was also observed that for $Re_H = 10$ there was a symmetric behavior of $(H_1/L_1)_o$, while for numbers of $Re_H > 10$, the behavior becomes asymmetrical, due to the effect of the primary vortex on the flow.

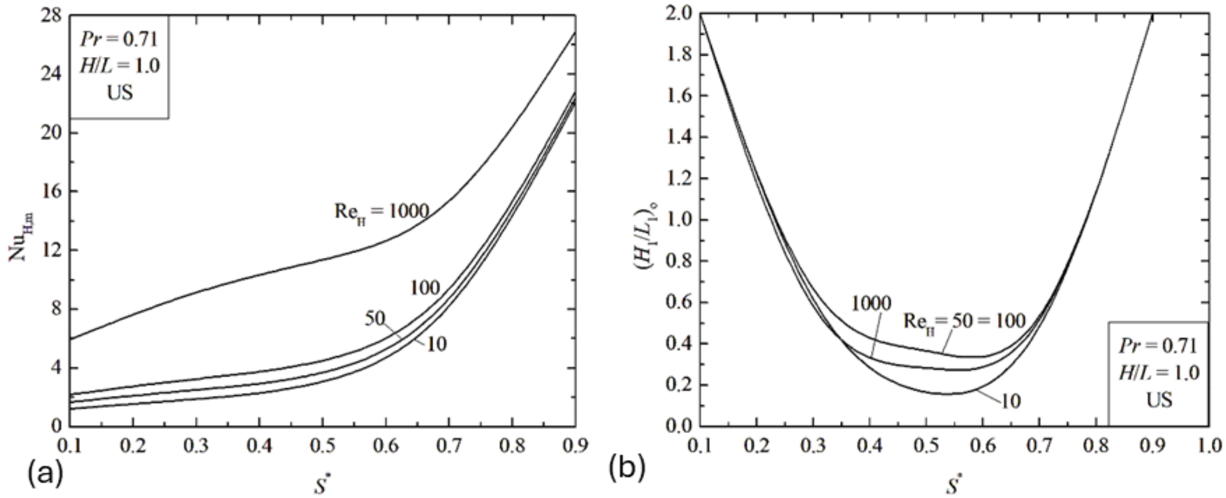

Fig. 18 – Effect of distance S^* for a rectangular fin placed at the upstream surface on: a) the once maximized Nusselt number, $Nu_{H,m}$, b) once optimized ratio H_1/L_1, $(H_1/L_1)_o$.

4.4 Comparisons and summary of the optimal fin geometries and positions

Fig. 19 shows the relation within the twice maximized Nusselt number, $Nu_{H,mm}$, and the Re_H for the fin mounted in the three different surfaces of the cavity. It is clear that the increase of Re_H leads to augmentation of $Nu_{H,mm}$. The $Nu_{H,mm}$ evaluated for the fin mounted on the cavity's upstream and downstream surfaces presented similar results. The $Nu_{H,mm}$ values are slightly higher when the fin was mounted on the downstream surface, indicating that flow has more access to remove the heat from the fin in this configuration. On the contrary the Nusselt number drops by almost half once the fin was positioned at the bottom of the cavity. It is explained by the difficulty for the flow to penetrate in the *y*-direction on the cavity to remove heat compared to the fin positioned on the upstream or downstream surfaces.

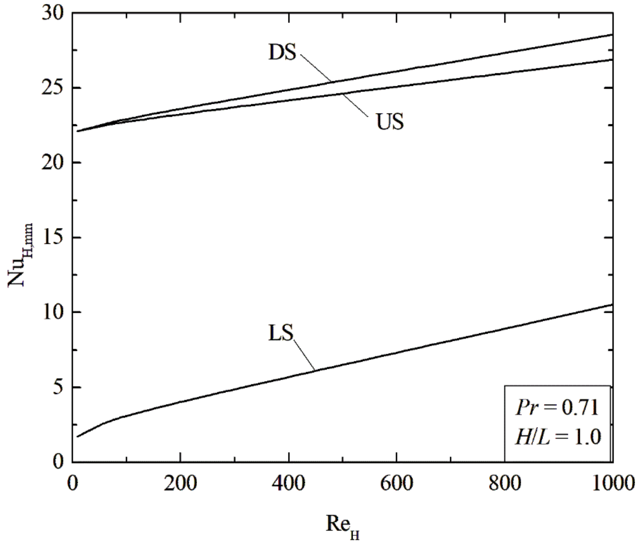

Fig. 19 – Effect of the Reynolds number (Re_H) over the twice maximized Nusselt number ($Nu_{H,mm}$).

Fig. 20 presents the best positions for the fins inserted on the upstream, downstream and lower surfaces of the cavity (a) and the aspect ratio of the fin twice optimized $(H_1/L_1)_{oo}$ (b) in relation to Re_H. In Fig. 20a, the results show that the best position for the fins inserted on the cavity's upstream and downstream sides is the same, $(S^*)_o = 0.9$, close to the top of the cavity. It is attributed to the proximity of the fin to the imposed fluid flow. In addition, in these cases, the fluid flow has more access to the bottom and the side of the fin, improving the heat transfer and increasing the Nu_H. Once the fin was placed on the cavity's low surface, the best position was $(S^*)_o = 0.5$, in the middle of the cavity. When the fin is positioned at the beginning or end of the cavity at the lower surface, fluid flow is usually trapped between the right or left side of the fin and the surface of the cavity, decreasing the heat transfer in these spots. From Fig 20b, it is possible to observe the same trend of results for the fins inserted in the upstream and downstream surfaces with a twice optimized fin geometry that remained constant with $(H_1/L_1)_{oo} = 2.0$, which conducted the upper fin surface the most close possible of the lid-driven cavity surface. For the fin inserted in the lower surface of the cavity there was a decrease of $(H_1/L_1)_{oo}$ when Reynolds number increases. The optimal ratio geometry obtained for this configuration was $(H_1/L_1)_o = 0.4$.

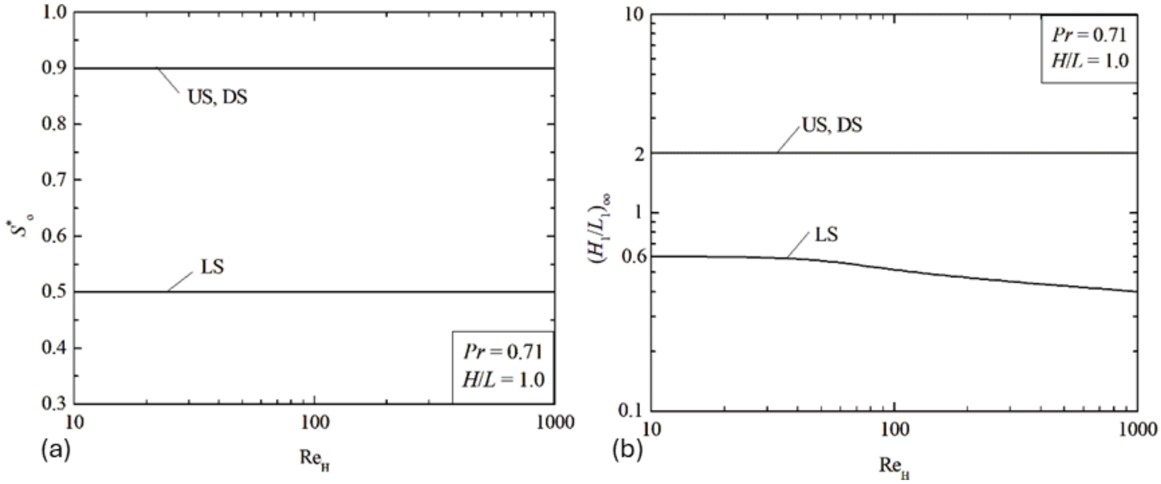

Fig. 20 – Effect of Reynolds number (Re_H) over optimal shapes reached in Fig. 19: a) $(S^*)_o$, b) $(H_1/L_1)_{oo}$.

Finally, Fig. 21 presents the temperature field for the optimal fin shape at $Re_H = 1000$ for the fin placed at (a) downstream, (b) low and (c) upstream surface of the cavity. It is clear from the figure that the twice maximized Nusselt number was significantly higher when the fin was placed on the cavity's downstream surface. The fin placed on the downstream surface with $(H_1/L_1)_{oo} = 2.0$ improved Nu_H about 63.15% and 5.85% in relation to the fin positioned in the lower and upstream surfaces, respectively.

Overall, the results indicated that there is no universal position for the mounted fin that results to the best system performance. Furthermore, even the surface area for the fin with $(H_1/L_1) = 10.0$ being higher than for the optimum shape $(H_1/L_1)_{oo} = 2.0$, the best geometry that presented the highest Nu_H was achieved by a fin geometry with a lower surface area. The difference of the Nusselt numbers between the best and worst configurations is much higher than the surface area of the fin. In other words, increasing the surface area does not necessarily lead to the most efficiency system. The results presented in this work reinforce the importance of using the Constructal Design Method to study forced convection heat transfer problems to obtain the optimal geometries for a given problem.

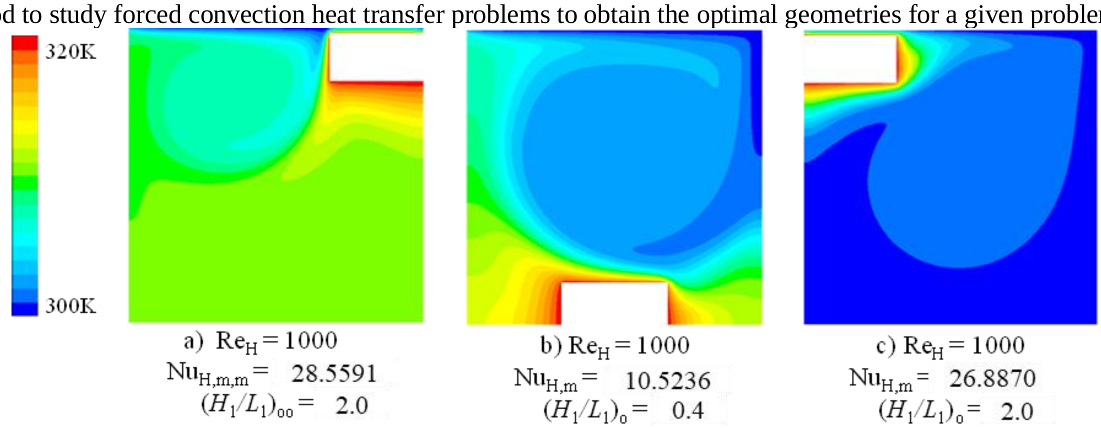

Fig. 21 – Temperature maps for the optimal shapes when Re_H = 1,000 for different placements of heated blocks on the cavity surfaces: a) downstream, b) lower, and c) upstream surface.

5. Conclusions

This work aimed to numerically investigate the influence of the rectangular fin geometry mounted on different surfaces and positions of lid-driven square cavities under laminar forced convective flows. The Constructal Design method was applied for the geometrical assessment of the fin geometry. The study was carried out for four Re_H: 10, 50, 100, and 1000 over the Nusselt number for a fluid flow with a fixed Pr = 0.71 for different fin geometries and with the rectangular fins being positioned on the lower, upstream and downstream surfaces of the cavity. The ratio between the area filled by the fin and the cavity area was considered fixed (φ = 0.05), and the geometry had two degrees of freedom: H_1/L_1 and S^*.

The findings of this work revealed that the fin shape had an important impact on the Nusselt number. The constructal design method considerably improved thermal performance for all the cases studied. For Re_H = 1000, the best results were for the fin inserted in the downstream surface with $(H_1/L_1)_{oo}$ = 2.0 and S^*=0.9, which increased Nu_H by 63.15% compared to the fin inserted in the lower surface and about 5.85% compared to the fin positioned in the upstream surface. It was also noted that the twice optimized $(H_1/L_1)_{oo}$ ratio was the same for the fins inserted on the side surfaces of the cavity, even the fluid flow (mainly the main vortex) being different on the side surfaces of the cavity. Additionally, the $(H_1/L_1)_{oo}$ ratio obtained for the fin inserted on the low surface differed from those obtained on the side surfaces of the cavity. It indicates that the fin geometry needs to be adapted according to the surface of the cavity where it is inserted. Finally, the results showed that the position of the fin affected the H_1/L_1 ratio over the Nu_H regardless of the surface where the cavity was inserted. For fins inserted on the lower surface of the cavity, it was found that the best thermal performance was obtained for the intermediate S^* and small H_1/L_1 ratios. On the other hand, when the fin was mounted on the lateral surfaces of the cavity, the highest S^* = 0.9 and the lowest H_1/L_1 = 2.0 (for S^* = 0.9) led to the best thermal performances, considering the Nu_H as the performance indicator.

Acknowledgments

The author E. S. Aldrighi thanks CAPES for Master Science scholarship (Finance code 001). The author G.D. Telli thanks FAPERGS for the financial support (Process: 23/2551-0000802-5). The authors F.S.F. Zinani, L.A. Isoldi, L.A.O. Rocha and E.D. dos Santos thank CNPq for research grant (Processes: 311444/2021-0, 309648/2021-1, 307791/2019-0, and 308396/2021-9).

References

[1] A. H. Jabado, M. El Hassan, H. H. Assoum, A. Hammoud, K. A. Meraim, A. Sakout, A review of cavity heat transfer under separated/reattached flow conditions, *Energy Reports*, Vol. 8, pp. 949-956, 2022.

[2] S. Gupta, A. Chauhan, C. Sasmal, Influence of elastic instability and elastic turbulence on mixed convection of viscoelastic fluids in a lid-driven cavity, *International Journal of Heat and Mass Transfer*, Vol. 186, pp. 122469-122469, 2022.

[3] E. D. Dos Santos, G. L. Piccoli, F. H. R. França, A. P. Petry, Analysis of mixed convection in transient laminar and turbulent flows in driven cavities, *International Journal of Heat and Mass Transfer,* Vol. 54, No. 21-22, pp. 4585-4595, 2011.

[4] M. A. Ismael, I. Pop, A. J. Chamkha, Mixed convection in a lid-driven square cavity with partial slip, *International Journal of Thermal Sciences*, Vol. 82, No. 1, pp. 47-61, 2014.

[5] P. M. Rodrigues, C. Biserni, C. C. de Escobar, L. A. O. Rocha, L. A. Isoldi, E. D. dos Santos, Geometric optimization of a lid-driven cavity with two rectangular intrusions under mixed convection heat transfer: A numerical investigation motivated by constructal design, *International Communications in Heat and Mass Transfer*, Vol. 117, No. July, pp. 104759-104759, 2020.

[6] R. Iwatsu, J. M. Hyun, K. Kuwahara, Mixed convection in a driven cavity with a stable vertical temperature gradient, *International Journal of Heat and Mass Transfer*, Vol. 36, No. 6, pp. 1601-1608, 1993.

[7] M. Sheikholeslami, S. A. Shehzad, F. M. Abbasi, Z. Li, Nanofluid flow and forced convection heat transfer due to Lorentz forces in a porous lid driven cubic enclosure with hot obstacle, *Computer Methods in Applied Mechanics and Engineering*, Vol. 338, pp. 491-505, 2018.

[8] M. F. Karim, S. Islam, M. M. Rahman, A. Paul, G. Mandal, A numerical investigation on forced convection heat and mass transfer performance in a right triangular cavity, *International Journal of Thermofluids*, Vol. 21, No. January, pp. 100578-100578, 2024.

[9] T. S. Cheng, W. H. Liu, Effect of temperature gradient orientation on the characteristics of mixed convection flow in a lid-driven square cavity, *Computers & Fluids,* Vol. 39, No. 6, pp. 965-978, 2010.

[10] K. M. Gangawane, H. F. Oztop, M. E. Ali, Mixed convection in a lid-driven cavity containing triangular block with constant heat flux: Effect of location of block, *International Journal of Mechanical Sciences,* Vol. 152, No. August 2018, pp. 492-511, 2019.

[11] M. A. Alomari, K. Al-Farhany, Q. H. Al-Salami, I. R. Ali, N. Biswas, M. H. Mohamed, F. Alqurashi, Numerical analysis to investigate the effect of a porous block on MHD mixed convection in a split lid-driven cavity with nanofluid, *International Journal of Thermofluids,* Vol. 22, pp. 100621-100621, 2024.

[12] M. K. Moallemi, K. S. Jang, Prandtl number effects on laminar mixed convection heat transfer in a lid-driven cavity, *International Journal of Heat and Mass Transfer,* Vol. 35, No. 8, pp. 1881-1892, 1992.

[13] A. K. Prasad, J. R. Koseff, Combined forced and natural convection heat transfer in a deep lid-driven cavity flow, *International Journal of Heat and Fluid Flow,* Vol. 17, No. 5, pp. 460-467, 1996.

[14] S. Sivasankaran, V. Sivakumar, A. K. Hussein, Numerical study on mixed convection in an inclined lid-driven cavity with discrete heating, *International Communications in Heat and Mass Transfer,* Vol. 46, pp. 112-125, 2013.

[15] T. P. Chiang, W. H. Sheu, R. R. Hwang, Effect of Reynolds number on the eddy structure in a lid-driven cavity, *International Journal for Numerical Methods in Fluids,* Vol. 26, No. 5, pp. 557-579, 1998.

[16] S. E. Ahmed, Z. Raizah, A. A. M. Arafa, S. A. Hussein, FEM treatments for MHD highly mixed convection flow within partially heated double-lid driven odd-shaped enclosures using ternary composition nanofluids, *International Communications in Heat and Mass Transfer,* Vol. 145, pp. 106854-106854, 2023.

[17] A. J. Chamkha, S. H. Hussain, Q. R. Abd-Amer, Mixed convection heat transfer of air inside a square vented cavity with a heated horizontal square cylinder, *Numerical Heat Transfer; Part A: Applications,* Vol. 59, No. 1, pp. 58-79, 2011.

[18] H. F. Oztop, Z. Zhao, B. Yu, Fluid flow due to combined convection in lid-driven enclosure having a circular body, *International Journal of Heat and Fluid Flow,* Vol. 30, No. 5, pp. 886-901, 2009.

[19] N. S. Gibanov, M. A. Sheremet, H. F. Oztop, K. Al-Salem, Convective heat transfer in a lid-driven cavity with a heat-conducting solid backward step under the effect of buoyancy force, *International Journal of Heat and Mass Transfer,* Vol. 112, pp. 158-168, 2017.

[20] K. Khanafer, S. M. Aithal, Mixed convection heat transfer in a lid-driven cavity with a rotating circular cylinder, *International Communications in Heat and Mass Transfer,* Vol. 86, pp. 131-142, 2017.

[21] S. E. Ahmed, M. Alhazmi, Impacts of the rotation and various thermal conditions of cylinders within lid-driven enclosures filled with glass balls in the presence of radiation: FEM simulation, *International Communications in Heat and Mass Transfer,* Vol. 128, pp. 105603-105603, 2021.

[22] A. K. Kareem, S. Gao, A comparison study of mixed convection heat transfer of turbulent nanofluid flow in a three-dimensional lid-driven enclosure with a clockwise versus an anticlockwise rotating cylinder, *International Communications in Heat and Mass Transfer,* Vol. 90, pp. 44-55, 2018.

[23] H. Moayedi, N. Amanifard, H. M. Deylami, A comparative study of the effect of fin shape on mixed convection heat transfer in a lid-driven square cavity, *Journal of the Brazilian Society of Mechanical Sciences and Engineering,* Vol. 44, No. 8, pp. 1-19, 2022.

[24] A. Bejan, Constructal-theory network of conducting paths for cooling a heat generating volume, *International Journal of Heat and Mass Transfer,* Vol. 40, No. 4, pp. 799-811, 1997.

[25] A. Bejan, 2000, *Shape and structure, from engineering to nature*, Cambridge university press,

[26] A. Bejan, J. P. Zane, 2013, *Design in Nature: How the Constructal Law governs evolution in biology, physics, technology, and social organizations*, Anchor,

[27] A. Bejan, S. Lorente, 2008, *Design with Constructal Theory*, John Wiley & Sons, Inc., Hoboken, NJ, USA

[28] A. Bejan, S. Lorente, The constructal law and the evolution of design in nature, *Physics of Life Reviews,* Vol. 8, No. 3, pp. 209-240, 2011.

[29] S. Lorente, A. Bejan, Current trends in constructal law and evolutionary design, *Heat Transfer-Asian Research,* Vol. 48, No. 8, pp. 3574-3589, 2019.

[30] A. Bejan, S. Lorente, Constructal law of design and evolution: Physics, biology, technology, and society, *Journal of Applied Physics,* Vol. 113, No. 15, pp. 151301-151301, 2013.

[31] S. Lorente, M. Hautefeuille, A. Sanchez-Cedillo, The liver, a functionalized vascular structure, *Scientific Reports,* Vol. 10, No. 1, pp. 16194-16194, 2020.

[32] X. Zhang, S. Lorente, The growth of capillary networks by branching for maximum fluid access, *Scientific Reports,* Vol. 13, No. 1, pp. 1-10, 2023.

[33] S. Lorente, A. Bejan, J. L. Niu, Phase change heat storage in an enclosure with vertical pipe in the center, *International Journal of Heat and Mass Transfer,* Vol. 72, pp. 329-335, 2014.

[34] S. Lorente, A. Bejan, J. L. Niu, Constructal design of latent thermal energy storage with vertical spiral heaters, *International Journal of Heat and Mass Transfer,* Vol. 81, pp. 283-288, 2015.

[35] S. Gungor, E. Cetkin, S. Lorente, Canopy-to-canopy liquid cooling for the thermal management of lithium-ion batteries, a constructal approach, *International Journal of Heat and Mass Transfer,* Vol. 182, pp. 121918-121918, 2022.

[36] G. D. Telli, S. Gungor, S. Lorente, Counterflow canopy-to-canopy and U-turn liquid cooling solutions for battery modules in stationary Battery Energy Storage Systems, *Applied Thermal Engineering,* Vol. 238, No. July 2023, pp. 121997-121997, 2024.

[37] L. Chen, H. Feng, F. Zhang, Y. Ge, Constructal design for composite heat dissipating structure composed of an "arrow"-shaped high conductivity channel and an externally connected "T"-shaped fin, *International Communications in Heat and Mass Transfer,* Vol. 153, No. March, pp. 107341-107341, 2024.

[38] C. L. Zhu H, Feng H, Ge Y, Constructal design of comb-shaped high thermal conductivity channel in a stacked chip, *International Communications in Heat and Mass Transfer,* Vol. 155, No. 107557, 2024.

[39] X. Z. Lu Z, Xi K, Lin D, Liu H, Ge Y, Wu F, Constructal evolutionary design of liquid cooling heat sink embedded in 3D-IC based on deep neural network prediction, *International Communications in Heat and Mass Transfer,* Vol. 152, No. 107273, 2024, 2024.

[40] G. Lorenzini, B. S. Machado, L. A. Isoldi, E. D. dos Santos, L. A. O. Rocha, Constructal Design of Rectangular Fin Intruded Into Mixed Convective Lid-Driven Cavity Flows, *Journal of Heat Transfer,* Vol. 138, No. 10, pp. 1-12, 2016.

[41] E. S. Aldrighi, P. M. Rodrigues, B. D. D. A. Rodriguez, L. A. Isoldi, L. A. O. Rocha, E. D. Dos Santos, Constructal design of rectangular fin intruded into different surfaces of forced convective lid-driven cavity flow, *International Journal of Fluid Mechanics Research,* Vol. 43, No. 5-6, pp. 418-440, 2016.

[42] A. L. Razera, R. J. C. da Fonseca, L. A. Isoldi, E. D. dos Santos, L. A. O. Rocha, C. Biserni, Constructal design of a semi-elliptical fin inserted in a lid-driven square cavity with mixed convection, *International Journal of Heat and Mass Transfer,* Vol. 126, pp. 81-94, 2018.

[43] R. da Silveira Borahel, F. S. F. Zinani, L. A. O. Rocha, E. D. dos Santos, L. A. Isoldi, C. Biserni, Geometric optimization of a rectangular isothermal block inside a lid-driven cavity by means of constructal design, *International Communications in Heat and Mass Transfer,* Vol. 139, pp. 106499-106499, 2022.

[44] A. Bejan, 2013, *Convection heat transfer*, John Wiley & Sons, Inc, New Jersey, 4thed.

[45] W. M. H.K. Versteeg, 2007, *An Introduction to Computational Fluid Dynamics: The Finite Volume Method*, Pearson Education,

[46] S. V. Patankar, 2018, *Numerical Heat Transfer and Fluid Flow*, CRC Press, Boca Raton

[47] R. P. Maciel, P. H. Oleinik, E. D. Dos Santos, L. A. O. Rocha, B. N. Machado, M. d. N. Gomes, L. A. Isoldi, Constructal Design Applied to an Oscillating Water Column Wave Energy Converter Device under Realistic Sea State Conditions, *Journal of Marine Science and Engineering,* Vol. 11, No. 11, pp. 1-31, 2023.

[48] M. Nallasamy, K. K. Prasad, On cavity flow at high Reynolds numbers, *Journal of Fluid Mechanics,* Vol. 79, No. 2, pp. 391-414, 1977.